

Changes in productivity and intermediate circulation in the northern Indian Ocean since the last deglaciation: new insights from benthic foraminiferal Cd/Ca records and benthic assemblage analyses

Ruifang Ma^{1,2*}, Sophie S epulcre¹, Laetitia Licari³, Fr ed eric Haurine¹, Franck Bassinot⁴,
Zhaojie Yu⁵, Christophe Colin¹

¹ GEOPS, Universit  Paris-Saclay, CNRS, Orsay, 91405, France.

² State Key Laboratory of Cryospheric Science, Northwest Institute of Eco-Environment and Resources, Chinese Academy of Sciences, Lanzhou, 730000, China.

³ CEREGE, Aix-Marseille Universit -Europe de l'Arbois-BP80, Aix-en-Provence, 13545, France.

⁴ LSCE/IPSL, CEA CNRS UVSQ, Gif Sur Yvette, F-91190, France.

⁵ Key Laboratory of Marine Geology and Environment, Institute of Oceanology, Chinese Academy of Sciences, Qingdao, 266071, China.

*Correspondence to: R. MA (maruifang89@hotmail.com)

Abstract. We have measured Cd/Ca ratios of several benthic foraminiferal species and studied benthic foraminiferal assemblages on two cores from the northern Indian Ocean (Arabian Sea and northern Bay of Bengal, BoB), in order to reconstruct variations in intermediate water circulation and paleo-nutrient content since the last deglaciation. Intermediate water Cd_w records estimated from the benthic Cd/Ca reflect past changes in surface productivity and/or intermediate-bottom water ventilation. The benthic foraminiferal assemblages are consistent with the geochemical data. These results suggest that during the last deglaciation, Cd_w variability was primarily driven by changes in intermediate water properties, indicating an enhanced ventilation of intermediate-bottom water masses during both Heinrich Stadial 1 and Younger Dryas (HS1 and YD, respectively). During the Holocene, however, surface primary productivity appeared to have influenced Cd_w more than intermediate water mass properties. This is evident during the early Holocene (from 10 to 6 cal kyr BP) when benthic foraminiferal assemblages indicate that surface primary productivity was low, resulting in low intermediate water Cd_w at both sites. Then, from ~ 5.2 to 2.4 cal kyr BP, surface productivity increased markedly, causing a significant increase in the intermediate water Cd_w in the southeastern Arabian Sea and the northeastern BoB. The comparison of intermediate water Cd_w records with previous reconstructions of past Indian monsoon evolution during the Holocene suggests a direct control of intermediate water Cd_w by monsoon-induced changes in upper water stratification and surface primary productivity.

1. Introduction

During the last deglaciation, a two-step rapid increase in atmospheric CO_2 occurred during the 17-13.8 and 12.3-11.2 cal kyr BP time intervals (e.g., Monnin et al., 2001). Several studies suggest that variations in the Southern Ocean circulation contributed to these increases in atmospheric CO_2 by transferring deep ocean carbon to the upper ocean and atmosphere, through enhanced upwelling and increased northward penetration of the Antarctic Intermediate Water (AAIW) in all ocean basins (e.g., Marchitto et al., 2007; Anderson et al., 2009; Skinner et al., 2014). Different proxies have been used to reconstruct past changes in intermediate circulation,

41 such as radiocarbon activity ($\Delta^{14}\text{C}$) (e.g., Marchitto et al., 2007; Bryan et al., 2010), benthic $\delta^{13}\text{C}$ (e.g., Pahnke
42 and Zahn, 2005; Jung et al., 2009; Ma et al., 2019), foraminiferal ϵ_{Nd} (e.g., Pahnke et al., 2008; Xie et al., 2012;
43 Yu et al., 2018) and benthic foraminifera Sr/Ca (Ma et al., 2020). These studies have focused on the close
44 relationship between enhanced ventilation in the Southern Ocean and rising atmospheric CO_2 during the last
45 deglaciation period. Furthermore, it has been shown that glacial-interglacial transfer of CO_2 between the oceans
46 and the atmosphere could also be linked to changes in the efficiency of the oceanic biological pump (Pichevin et
47 al., 2009; Ziegler et al., 2013; Bauska et al., 2016; Hertzberg et al., 2016; Jaccard et al., 2016; Yu et al., 2019),
48 which may contribute to up to half of the observed CO_2 flux (Kohfeld, 2005).

49 The oceanic biological pump and nutrient upwelling are at least partly controlled by intermediate-deep water
50 circulation, contributing to the observed CO_2 changes (e.g., Toggweiler, 1999; Marchitto and Broecker, 2006).
51 To track past changes in the nutrient concentration of intermediate water masses, benthic foraminifera Cd/Ca has
52 been used in many recent studies (e.g., Came et al., 2008; Poggemann et al., 2017; Valley et al., 2017; Umling et
53 al., 2018); indeed, the benthic foraminifera Cd/Ca is a robust proxy of seawater cadmium concentrations (Cd_w)
54 (Boyle, 1988; 1992), which shows a positive linear correlation with labile nutrients (phosphate and nitrate) in the
55 modern ocean (e.g., Boyle et al., 1976; Boyle, 1988; Elderfield and Rickaby, 2000). The benthic foraminifera
56 incorporate Cd as a function of Cd_w with a species-dependent partition coefficient (e.g., Tachikawa and
57 Elderfield, 2002). Thus, the Cd measured in the fossil tests reflects the paleo-nutrient concentrations of the
58 surrounding water masses, and can be used to investigate past changes in intermediate-to-deep ocean properties
59 (e.g., Boyle and Keigwin, 1982; Oppo and Fairbanks, 1987; Came et al., 2008; Poggemann et al., 2017; Valley et
60 al., 2017; Umling et al., 2018).

61 Complementary to the geochemical proxies, the type of benthic foraminifers and their abundance, both of
62 which are related to organic flux and ecosystem oxygenation, make benthic foraminifer assemblages a powerful
63 proxy for estimating past variations in bottom water conditions (e.g., Corliss et al., 1986; Schmiedl et al., 1998;
64 Almogi-Labin et al., 2000) in conjunction with organic matter fluxes to the seafloor (e.g., Altenbach et al., 1999;
65 Van der Zwaan et al., 1999; Fontanier et al., 2002; Caille et al., 2015). Benthic foraminifera have been
66 successfully used as indicators of surface productivity, especially in high carbon flux regions (Schnitker, 1994).
67 By comparing past benthic foraminiferal assemblages to modern ones, changes in food supply and oxygen
68 concentrations of the bottom water can be reconstructed (e.g., Corliss, 1979; Peterson, 1984; Murgese and De
69 Deckker, 2005). Recently, the combining of benthic foraminiferal assemblages and geochemical proxies has
70 received increasing attention and have been used to reconstruct the evolution of surface productivity and
71 upwelling intensity in the Indian Ocean (e.g., Hermelin 1991, 1992; Hermelin and Shimmield, 1995; Den Dulk
72 et al., 1998; Murgese and De Deckker, 2005).

73 The Arabian Sea is one of the most productive regions of the ocean today (Banse, 1987; Marra and Barber,
74 2005). Surface productivity is dominated by the monsoon system, which has a strong impact on the distribution
75 and dynamics of stratification and vertical mixing (Lévy et al., 2007). Numerous studies have focused on the
76 reconstruction of the paleo-productivity of the Arabian Sea in relation to past changes in monsoon intensity (e.g.,
77 Prell and Kutzbach, 1987; Naidu and Malmgren, 1996; Gupta et al., 2003; Singh et al., 2006; 2011; Bassinot et
78 al., 2011; Saraswat et al., 2014). By contrast, little is known about the paleoproductivity of the BoB, especially
79 its links to changes in monsoon precipitation (Phillips et al., 2014; Zhou et al., 2020). Consequently, studying
80 paleoproductivity and past nutrient concentration of intermediate water masses in the northeastern Indian Ocean

81 will also allow us to completely understand the influence of monsoon climate changes in tropical ocean ecology
82 at different timescales. Besides, as the benthic foraminiferal Cd/Ca is a promising proxy to reconstruct the
83 intermediate-deep water nutrient content (e.g., Boyle and Keigwin, 1982; Tachikawa and Elderfield, 2002; Came
84 et al., 2008; Poggemann et al., 2017; Valley et al., 2017), most of the studies referred to above have
85 reconstructed deep-intermediate water masses in the past (e.g., Came et al., 2008; Bryan and Marchitto, 2010;
86 Poggemann et al., 2017; Valley et al., 2017), and only few works investigate the relationship between the
87 intermediate water masses nutrient and surface productivity (Bostock et al., 2010; Olsen et al., 2016).
88 Furthermore, the evolution of the nutrient content of intermediate water masses since the last deglaciation has
89 never been reconstructed in the Indian Ocean, where only two low-resolution Cd/Ca records are available for
90 deep-water depths (Boyle et al., 1995), and, to our knowledge, none are available for intermediate water depths.

91 In this study, we provide, for the first time, two benthic foraminifera Cd/Ca records at intermediate water
92 depths in the northern Indian Ocean (Arabian Sea and northern Bay of Bengal). These data make it possible to
93 estimate past changes in the nutrient content since the last deglaciation. We have also investigated benthic
94 foraminiferal assemblages obtained from core MD77-191 (southeastern Arabian Sea) to help us reconstructing
95 the conditions at the seafloor. Combined with planktonic foraminiferal $\delta^{18}\text{O}$, benthic $\delta^{13}\text{C}$, and Cd/Ca records
96 obtained from the same core, as well as with results already published in the Bay of Bengal (Ma et al., 2019;
97 2020), this study aims to document past variations in intermediate- and deep-water conditions and to decipher
98 their links with surface paleo-productivity and intermediate water ventilation.

99

100 **2. Material and modern hydrological setting**

101

102 We analyzed sediment core MD77-191 (07°30'N-76°43'E, 1254m) located in the Arabian Sea (off the
103 southern tip of India), and core MD77-176 (14°30'5N-93°07'6E, 1375m) retrieved in the northeastern Bay of
104 Bengal (BoB). These cores were collected in 1977 during the OSIRIS III cruise of the French N/O Marion
105 Dufresne (Fig. 1).

106 The age model of core MD77-191 was established by using accelerator mass spectrometry (AMS) ^{14}C dates
107 obtained on 9 monospecific samples of planktonic foraminifera *Globigerinoides bulloides* (Bassinot et al., 2011),
108 one sample of pteropods (Mlénéck, 1997), and three samples of the planktonic foraminifera *Globigerinoides*
109 *ruber* (Ma et al., 2020). The average sedimentation rate of core MD77-191 is about 53 cm/kyr and up to 90
110 cm/kyr during the Holocene, providing a high-resolution, continuous record since 17 cal kyr BP.

111 The age model of core MD77-176 was previously established by using 31 planktonic foraminifer (*G. ruber*)
112 AMS ^{14}C dates combined with the core MD77-176 oxygen isotope record obtained on planktonic foraminifera *G.*
113 *ruber*, which were correlated to the GISP2 Greenland ice core record (Marzin et al., 2013). Core MD77-176
114 displays high accumulation rates (average ~25 cm/kyr and up to 40 cm/kyr during the Holocene).

115 In the modern ocean, the surface waters of the Arabian Sea and BoB are characterized by seasonally reversing
116 currents that are driven by the monsoon winds (Fig1.a). The surface water masses shallower than 150 m in the
117 Arabian Sea are mainly Arabian Sea High Salinity Water (ASHS, 36.5 psu) (Talley et al., 2011). In the BoB, the
118 surface waters above 100 m are designated Bay of Bengal surface waters (BoBSW), which have a low salinity
119 (31 psu) due to large river inputs (Talley et al., 2011). Today, the northward extension of AAIW in the Indian
120 Ocean rarely reaches beyond 10°S (Lynch-Stieglitz et al., 1994). The sites of cores MD77-191 and MD77-176

121 are mainly bathed, therefore, by the North Indian Intermediate Water (Olson et al., 1993; Reid, 2003) with a
122 potential contribution from the Red Sea Outflow Water (RSOW) for the site MD77-191 (Beal et al., 2000).

123 Due to the land-sea configuration in the north by Asia, the deep waters of the northern Indian Ocean originate
124 from the south, including the Circumpolar Deep Water (CDW) and North Atlantic Deep Water (NADW) (You,
125 2000; Tomczak and Godfrey, 2003; Talley et al., 2011). Thus, between 1500 and 3800m, the dominant deep
126 water in the North Indian Ocean is Indian Deep Water (IDW), originating from the CDW admixed with NADW
127 (You, 2000; Tomczak and Godfrey, 2003; Talley et al., 2011). Then, during their pathway, the bottom water
128 upwells when it expands northward in northern Indian Ocean, returning to shallower depths (You, 2000, Figure
129 1c). Therefore, variations of deep-water masses can also influence the intermediate-depth waters in the northern
130 Indian Ocean.

131 As far as surface waters are concerned, during the summer monsoon, the clockwise circulation in the
132 Arabian Sea drives high salinity waters from the northern to the southeastern Arabian Sea. By contrast, during
133 the winter monsoon, the northeastern winds bring low salinity water (BoBSW) from the BoB. The northern
134 Indian Ocean, especially the Arabian Sea, is characterized by highly variable seasonal productivity (Shankar et
135 al., 2002). Southwest winds during the summer season induce a strong Ekman pumping resulting in very active
136 upwelling along the western coasts of the Arabian Sea and thus promoting strong surface productivity (Shankar
137 et al., 2002; Fig. S1). By contrast, the surface productivity in the BoB is generally weak compared with the
138 Arabian Sea (e.g., Prasanna Kumar et al., 2001; Thushara and Vinayachandran, 2016; O'Malley, 2017; Fig. S1).
139 In the BoB, large river inputs of fresh water and direct monsoon precipitation lead to more stable stratification in
140 the upper ocean (Vinayachandran et al., 2002), and hence the vertical mixing of nutrients from the subsurface to
141 the euphotic zone is generally limited (Gomes et al., 2000). However, the primary productivity of the western
142 BoB shows a slight increase during the winter monsoon, as indicated by the distribution of chlorophyll in the
143 surface water (Thushara and Vinayachandran, 2016; O'Malley, 2017; Fig. S1).

144 Modern data indicate that the southern-sourced intermediate water (AAIW) in the Indian Ocean has a
145 phosphate concentration of about 2-2.5 $\mu\text{mol/kg}$ (Figs. 1b and c). In the Northern Intermediate Indian Ocean, the
146 phosphate concentration is significantly higher, ranging from 2.75 to 3 $\mu\text{mol/kg}$ in the Arabian Sea during the
147 summer monsoon, and from 2.5 to 2.75 $\mu\text{mol/kg}$ in the BoB during the winter monsoon (Figs. 1b and c). The
148 higher phosphate in the northern Indian Ocean can be linked to increased primary productivity (Banse, 1987;
149 Marra and Barber, 2005).

150

151 **3. Methods**

152 **3.1. Cd/Ca analysis**

153

154 In order to improve understanding of possible inter-species differences and microhabitat effects on the benthic
155 Cd/Ca records, we analyzed Cd/Ca in three calcite (*Cibicides pachyderma*, *Uvigerina peregrina*, and
156 *Globobulimina* spp.) and one aragonite (*Hoeglundina elegans*) benthic foraminiferal species from core MD77-
157 191. *C. pachyderma* is a shallow infaunal species, *U. peregrina* and *Globobulimina* spp. are endobenthic species
158 with intermediate and deep microhabitats, respectively (Fontanier et al., 2002). In core MD77-176, due to the
159 limitation of calcitic species, we only measured Cd/Ca ratios in *H. elegans* shells. Besides, Mn/Ca, Fe/Ca and
160 Al/Ca ratios were also measured in all benthic foraminiferal samples to check the robustness of Cd/Ca results
161 and the potential influence of contamination (i.e. oxides and sedimentary clay, Barker et al., 2003).

162 Each sample contained between 10 and 15 individuals picked from the 250-315 μm size fraction. Samples
163 were gently crushed, cleaned to remove clays, organic matter and elemental oxides by using reductive and
164 oxidative cleaning following previously published methods (Boyle and Keigwin, 1982; Barker et al., 2003).
165 Each sample was dissolved in 0.075N HNO_3 and analyzed using a single collector sector field high resolution
166 inductively coupled plasma mass spectrometer (HR-ICP-MS) Thermo Element XR hosted at the GEOPS
167 Laboratory (University Paris-Saclay, France).

168 The detailed instrumental settings and mother standard solutions are described in Ma et al., (2020). A blank
169 consisting of the same 0.1N HNO_3 used to dilute the standards and samples was also analyzed. We removed the
170 blank intensity values from all the raw intensities (including standards), and raw data were linearly drift-
171 corrected by interspersing a drift standard every four samples. Standard curves were used to calculate elemental
172 concentrations, coefficients of determination (r^2) always being >0.9999 for all elemental ratios. The mean
173 reproducibility and accuracy are 3.6% and 7.5%, respectively.

174

175 **3.2 Faunal analysis**

176

177 Benthic foraminiferal assemblages from core MD77-176 have already been published in Ma et al. (2019). For
178 core MD77-191, a total of 72 samples were collected for benthic foraminiferal assemblage determinations. In
179 each sample, benthic foraminifera ($>150\mu\text{m}$) were extracted, counted and identified to species level following
180 the taxonomical descriptions of various authors (e.g., Loeblich and Tappan, 1988; Jones, 1994; Holbourn et al.,
181 2013). For core MD77-191, there is no material left in this old, low diameter core and so we used samples
182 obtained earlier for stable isotope studies. Since the bulk weights of these samples were not recorded prior to
183 sieving, we could not perform the calculation of absolute abundance of foraminifera or accumulation rates. Thus,
184 we only converted the individual counts to percentages with respect to the total benthic foraminifera present in
185 each sample. In order to describe major faunal variations, we performed principal component analysis (PCA) on
186 the variance-covariance matrix using the PAST software (Version 3.0, Hammer et al., 2001). Species present
187 with a percentage $>1\%$ in at least 1 sample were used for statistical analysis and diversity calculation.

188

189 **4. Results**

190

191 **4.1. Elemental ratios results**

192

193 To check the influence of oxide contaminants on the elemental ratios, Mn/Ca was systematically measured.
194 The Mn/Ca of *H. elegans* from cores MD77-191 and MD77-176 ranges between 6.5-10 $\mu\text{mol/mol}$ and 1-30
195 $\mu\text{mol/mol}$, respectively. Such ranges are much lower than the 100 $\mu\text{mol/mol}$ limit proposed by Boyle (1983).
196 The Mn/Ca obtained on the three calcite benthic foraminifera species from core MD77-191 - *C. pachyderma* (5-
197 18 $\mu\text{mol/mol}$), *U. peregrina* (3-23 $\mu\text{mol/mol}$) and *Globobulimina* spp. (4-69 $\mu\text{mol/mol}$) - are also all below 100
198 $\mu\text{mol/mol}$ (Boyle, 1983). The Fe/Ca ratios are also lower than 1 mmol/mol in all samples from cores MD77-191
199 and MD77-176, in agreement with the limit proposed by Barker et al. (2003). In addition, Barker et al. (2003)
200 concluded that no significant pollution by clay minerals would be expected when Al/Ca is $<0.5 \text{ mmol/mol}$. In all
201 our samples, Al/Ca is below 0.5 mmol/mol , indicating that the sample cleaning procedure was efficient.

202 All of the above results indicate that our samples were not affected by contamination.

203

204 **4.1.1 Cd/Ca**

205
206 The Cd/Ca records of *C. pachyderma*, *U. peregrina* and *Globobulimina* spp. from core MD77-191 range
207 between 0.07-0.2 $\mu\text{mol/mol}$, 0.07-0.14 $\mu\text{mol/mol}$ and 0.03-0.09 $\mu\text{mol/mol}$, respectively (Fig. 2d; supplementary
208 Table S1).

209 The Cd/Ca records for the calcite benthic species *C. pachyderma* and *U. peregrina* have very low time
210 resolutions during the last deglaciation. However, some common patterns can be observed. The Cd/Ca records of
211 *C. pachyderma* and *U. peregrina* show lower values during the Heinrich stadial 1 (HS1, 17-15.2 cal kyr BP) and
212 Younger Dryas (YD, 13-11 cal kyr BP) cold periods, with average values of ~ 0.08 $\mu\text{mol/mol}$ for *C. pachyderma*
213 and ~ 0.09 $\mu\text{mol/mol}$ for *U. peregrina*. By contrast, these two species display higher Cd/Ca ratios (~ 0.12
214 $\mu\text{mol/mol}$) during the Bølling-Allerød warm period (B-A, 15-13.3 cal kyr BP) compared with the HS1 and YD.
215 Then, lower values (~ 0.1 $\mu\text{mol/mol}$ for *C. pachyderma*; 0.11 $\mu\text{mol/mol}$ for *U. peregrina*) are observed during the
216 early Holocene (10-5 cal kyr BP) compared to larger variations occurring in the late Holocene (5.2-2.4 cal kyr
217 BP). The Cd/Ca record of deep infaunal *Globobulimina* spp., obtained at a lower time resolution, shows different
218 variations compared with the two other taxa without any clear trend during the Holocene.

219 The *H. elegans* Cd/Ca values of core MD77-191 range from 0.05 to 0.31 $\mu\text{mol/mol}$ since 17 cal kyr BP (Fig.
220 2d; supplementary Table S1). Depleted values at about 0.07 $\mu\text{mol/mol}$ are recorded from the last deglaciation to
221 the early Holocene (17-5 cal kyr BP time interval). During the HS1 and the YD time intervals, a significant
222 decrease of about ~ 0.06 $\mu\text{mol/mol}$ occurred (even when taking into consideration the analytical error bar of
223 ± 0.02 , 2σ), and a slight increase (0.09 $\mu\text{mol/mol}$) is observed between 15 and 13.3 cal kyr BP (B-A period). A
224 rapid increase in the Cd/Ca values beginning at 5.2 cal kyr BP reaches a maximum (0.31 $\mu\text{mol/mol}$) during the
225 late Holocene.

226 For core MD77-176, the *H. elegans* Cd/Ca records range between 0.06 and 0.17 $\mu\text{mol/mol}$ over the past 18 cal
227 kyr BP (Fig. 2e; supplementary Table S1), without no clear trends and average benthic Cd/Ca values of ~ 0.09
228 $\mu\text{mol/mol}$ during the different periods (HS1, YD and Holocene). However, the benthic Cd/Ca record during the
229 Holocene seems to exhibit a slight increase both in value and range of variations after 6 cal kyr BP.

230

231 4.2. Foraminifera assemblages of core MD77-191

232

233 Benthic foraminiferal species richness ranges between 16 and 36, and the total abundance fluctuates between
234 82 and 642 specimens (supplementary Table S2). Hyaline species are the dominant constituents ($>80\%$), and
235 mainly consist of *Bulimina aculeata*, *H. elegans*, *C. pachyderma*, *Uvigerina* spp., *Gyroidina broeckhiana*,
236 *Globocassidulina subglobosa*, *Sphaeroidina bulloides*, *Gyroidinoides* spp., *Lenticulina* spp., *Melonis*
237 *barleeanum*, and *Globobulimina* spp. (including *Praeglobobulimina* spp.) (in decreasing order of relative
238 average abundance). Agglutinated taxa reach on average about 1.6%, and consist of *Textularia* sp.,
239 *Martinottiella communis*, and *Eggerella bradyi*. The average percentage of porcelaneous species, characterized
240 by *Pyrgo elongata*, *Pyrgo murrhina*, *Pyrgo depressa*, *Pyrgoella irregularis*, *Quinqueloculina* spp., *Sigmoilopsis*
241 *schlumbergeri*, and *Spiroloculina* spp., is about 5.1%.

242 Furthermore, we merged species that share an ecological similarity, such as *Globobulimina affinis*,
243 *Globobulimina pacifica*, and *Praeglobobulimina* spp. into *Globobulimina* spp. A total of 74 samples and 55
244 groups/species were adopted to perform principal component analysis (PCA) in order to identify major faunal
245 trends. The PCA analysis suggests that the benthic foraminifera could be grouped into three assemblages, with

246 PC1 (positive and negative loadings) and PC2 (positive loadings) representing 42 and 19% of the total variance,
247 respectively (Table 1). Besides, compared with the total variance of PC1 and PC2, PC3 is the largest one and
248 only explains 8% of the total variance for the rest PCs. The species composition consists of *H. elegans*,
249 *Globobulimina* spp. (Positive loadings), *Uvigerina peregrina*, *C. pachyderma* (Negative loadings) (Table 1). It
250 seems that the main composition of assemblages (PC3) is quite similar to PC1 and does not show more
251 information about the bottom conditions. Therefore, we only focus on the PC1 and PC2 in the manuscript for the
252 interpretation and do not present other PCs in the discussion.

253 Assemblage 1 can be defined as the combination of *Bulimina aculeata* and *C. pachyderma*, together with
254 *Pullenia bulloides* and *Ehrenbergina trigona* (Figs. 3 and S2) and display high positive PC1 loadings. This
255 assemblage dominated the foraminiferal record during the late Holocene (between 6 and 1.4 cal kyr BP).

256 By contrast, assemblage 2, dominated by *H. elegans* and *Bulimina manginata*, exhibits high negative PC1
257 loadings, and corresponds to the record during the early Holocene (Figs. 3 and S2). Other quantitatively
258 important contributors are *C. wuellerstorfi* and *Globocassidulina subglobosa* (Fig. S2).

259 Then, assemblage 3, dominated by *Sphaeroidina bulloides* and *Gyroidinoides orbicularis*, corresponds to the
260 positive loadings of PC2, which is more important during the last deglaciation (Figs. 3 and S2). The associated
261 species of assemblage 3 are *Bulimina mexicana* and *Gyroidinoides soldanii* (Fig. S2).

262 However, as the main composition of PC2 negative loadings is dominated by the same benthic species in
263 assemblages 1 and 2, it is difficult, therefore, to glean any additional information from this analysis. Thus, to
264 clarify the discussion, we prefer to use three assemblages in the following rather than the 2 PCs.

265

266 5. Discussion

267 5.1. Past intermediate water Cd_w concentrations from the Northern Indian Ocean

268

269 In the modern ocean, benthic foraminifera Cd/Ca shows a positive correlation with Cd_w and dissolved
270 nutrients (phosphate and nitrate) (Boyle et al., 1976; Hester and Boyle, 1982). As aragonitic benthic foraminifera
271 *H. elegans* faithfully records the bottom water Cd concentrations (Cd_w), Cd/Ca ratios can be converted to
272 seawater Cd_w with the appropriate relationship (Eq.1), where the partition coefficient $D_p \approx 1$ for all water depths
273 (Boyle et al., 1995; Bryan and Marchitto, 2010).

274

$$275 D_p = \frac{(Cd/Ca)_{foram}}{(Cd/Ca)_{water}} \quad (\text{Eq.1})$$

276

277 In contrast, the partition coefficient for calcite species changes with water depth. For water depths between
278 1150-3000 m, D_p was calculated based on the equation of Boyle, (1992; Eq. 2). The seawater Ca concentration is
279 assumed to be at a constant, mean value of 0.01 mol/kg (Boyle, 1992).

280

$$281 D_p = 1.3 + (\text{depth} - 1150) \times (1.6/1850) \quad (\text{Eq.2})$$

282

283 The intermediate Cd_w results based on the *H. elegans* Cd/Ca values of core MD77-191, range from 0.5 to 3.1
284 nmol/kg since 17 cal kyr BP (Fig. 4a), with a core top value of 0.80 nmol/kg in agreement with the estimated
285 intermediate water depth modern Cd_w (~0.83 nmol/kg) in the northern Indian Ocean (Boyle et al., 1995). The
286 intermediate Cd_w was also calculated from calcite benthic species *C. pachyderma*, *U. peregrina* and

287 *Globobulimina* spp. from core MD77-191, with values ranging between 0.53-1.48 $\mu\text{mol/mol}$, 0.52-1.04
288 $\mu\text{mol/mol}$ and 0.26-0.65 $\mu\text{mol/mol}$, respectively (Fig. 4a). The Cd_w values of *C. pachyderma* and *U. peregrina*
289 are within the same range. However, the *H. elegans* Cd_w values are higher than those from the two calcite
290 species, especially during the Late Holocene. Moreover, the core top data of *C. pachyderma* and *U. peregrina*
291 are also lower (~ 0.7 and 0.69 nmol/kg , respectively) than the modern estimated Cd_w data (~ 0.83 nmol/kg) in the
292 northern Indian Ocean (Boyle et al., 1995) (Fig. 4a). These depleted Cd_w values may be related to the benthic
293 foraminiferal microhabitat effect; indeed, *U. peregrina* is known to be strictly a shallow infaunal species, as well
294 as *C. pachyderma* (Fontanier et al., 2002), differing from strictly epifaunal taxa, such as *Cibicidoides*
295 *wuellerstorfi* (Mackensen et al., 1993).

296 Besides, the deep infaunal *Globobulimina* spp. Cd_w displays relatively much lower values and does not
297 exhibit strong variations compared to the other species investigated in this study, displaying a general increasing
298 trend from the last deglaciation to the Holocene. As *Globobulimina* spp. correspond to deep benthic infaunal
299 species, this result may indicate a stable nutrient content of pore water, as compared to other benthic taxa
300 associated with bottom water (Fig. 4a). Thus, when tracking past changes in the bottom water Cd_w
301 concentrations, the use of a strictly epifaunal species living at the water-sediment interface such as *H. elegans*
302 appears to be more robust than using endofaunal species that live in contact with pore water.

303 Relative variations in the Cd_w obtained from *C. pachyderma* and *U. peregrina* are in good agreement with the
304 records obtained on *H. elegans*. Variations of *H. elegans* Cd_w during the last deglaciation indicate a decrease of
305 about ~ 0.6 nmol/kg in the HS1 and YD periods, with a slight increase (0.9 nmol/kg) during the warm B-A. Cd_w
306 results from core MD77-191 indicate a shift from the last deglaciation (~ 0.7 nmol/kg) to the late Holocene
307 (~ 1.59 nmol/kg). During the Holocene, the Cd_w records display relatively low values of around 0.9 nmol/kg in
308 the 10-6 cal kyr BP time interval, and show a major shift at around 6.4 cal kyr BP with values rising up to 3.1
309 nmol/kg .

310 For core MD77-176, the intermediate water Cd_w calculated from the *H. elegans* Cd/Ca records ranges between
311 0.6 and 1.7 nmol/kg over the past 18 cal kyr BP (Fig. 4b). Compared with intermediate Cd_w from MD77-191, the
312 Cd_w record of core MD77-176 does not display any clear trend from the last deglaciation to the Holocene.
313 However, a slight increase is observed since 6 cal kyr BP, in agreement with the MD77-191 intermediate Cd_w
314 records. In addition, even though the MD77-176 record has a lower time resolution, it displays a shorter
315 maximum (1.3 nmol/kg) during the 13.4-11 cal kyr BP time interval.

316 To summarize, among the three calcite benthic taxa and the aragonitic benthic species *H. elegans*, the Cd/Ca
317 records of *H. elegans* appear to be the most suitable for tracking past Cd_w changes at intermediate water depth
318 through time. Thus, in the following discussion, we will only focus on the intermediate Cd_w calculated from the
319 *H. elegans* Cd/Ca from both studied cores.

320

321 **5.2. Comparison between geochemical records and benthic foraminiferal assemblages**

322

323 Comparing the geochemical records to the benthic assemblages, we can observe similar patterns. For core
324 MD77-191 from the southeastern Arabian Sea, three benthic assemblages were identified since the last
325 deglaciation. *S. bulloides* and *Gyroidinoides orbicularis* are major components of assemblage 3 (during the last
326 deglaciation), together with *B. mexicana* and *Gyroidinoides soldanii* (Figs. 3 and S2). *S. bulloides* and *B.*
327 *mexicana* are found in intermediate to high organic carbon flux rate regions (e.g., Schmiedl et al., 2000;

328 Eberwein and Mackensen, 2006, 2008), while *G. orbicularis* and *G. soldanii* are associated with well-
329 oxygenated and oligotrophic environments (Peterson, 1984; Burmistrova and Belyaeva, 2006; De and Gupta,
330 2010). Thus, assemblage 3 reflects mesotrophic environments and/or well-ventilated conditions during the last
331 deglaciation. Although millennial-scale changes in the benthic foraminiferal assemblages during the last
332 deglaciation could not be observed, benthic fauna 3 seems at least partly consistent with previous studies in the
333 northern Indian Ocean based on multiple geochemical proxies (e.g., benthic $\delta^{13}\text{C}$, intermediate water [CO_3^{2-}] and
334 ϵ_{Nd} records); these studies have revealed the presence of better-ventilated waters, which might correspond to
335 AAIW, during the HS1 and YD (e.g., Yu et al., 2018; Ma et al., 2019; 2020).

336 Benthic foraminiferal assemblage 2 predominates during the early Holocene and is characterized by *H.*
337 *elegans* and *B. manginata* as major contributors (Figs. 3 and S2). The other important contributors are *C.*
338 *wuellerstorfi* and *G. subglobosa*. *B. manginata* is found in high organic carbon flux rate conditions (De Rijk et
339 al., 2000; Eberwein and Mackensen, 2006, 2008). However, previous studies on *H. elegans*, *C. wuellerstorfi* and
340 *G. subglobosa* indicate that these species correspond to high levels of dissolved oxygen and oligotrophic settings
341 (e.g., Altenbach et al., 1999; Fontanier et al., 2002; Murgese and De Deckker, 2005, 2007; De and Gupta, 2010).
342 Periods dominated by these taxa probably indicate high oxygen levels and an oligotrophic environment. This is
343 consistent with previous studies in the area, based on benthic foraminiferal $\delta^{13}\text{C}$ and $\Delta^{14}\text{C}$ age difference (e.g.,
344 Naqvi et al., 1994; Bryan et al., 2010) (Fig. S3). Indeed, the glacial to Holocene benthic $\delta^{13}\text{C}$ shifts (0.35-0.4‰,
345 vs. PDB) at intermediate-deep water depth in the northern Indian Ocean are interpreted as reflecting an increased
346 contribution of better-ventilated deep water NADW in IDW, during the Holocene (e.g., Naqvi et al., 1994; Ma et
347 al., 2019) (Fig. S3). Furthermore, the increased B-P age offsets and depleted ϵ_{Nd} records obtained from the same
348 core site could also reflect the enhanced influence of NADW in IDW during the Holocene, which is
349 characterized by well-ventilated conditions and depleted nutrient concentrations (modern Cd_w , ~ 0.2 nmol/kg)
350 (Poggemann et al., 2017; Yu et al., 2018; Ma et al., 2019). The impact of this change in the IDW composition
351 can be recorded at intermediate-water depth since they are transformed to an upward flow during their pathway,
352 thus being a potential contribution to intermediate depth water masses (Naqvi et al., 1994; You, 2000). Although
353 the intermediate benthic $\delta^{13}\text{C}$ record from core MD77-191 is missing for the LGM, the average value for the
354 Holocene (~ 0.31 ‰, vs. PDB) is consistent with previous studies carried out in the northern Indian Ocean;
355 combined with the opposite trend between $\delta^{18}\text{O}_{\text{ivc}}$ records and intermediate water temperature from MD77-191
356 (Ma et al., 2020), all these records suggest well-ventilated conditions (Fig. S3). To summarize, the predominance
357 of benthic foraminifera assemblage 2 in the early Holocene seems to reflect better-ventilated water masses,
358 related to an enhanced contribution of NADW in IDW at the core site, as already observed in previous studies
359 (Poggemann et al., 2017; Yu et al., 2018; Ma et al., 2019; 2020).

360 By contrast, *B. aculeata* and *C. pachyderma* are major components of assemblage 1 (during the late Holocene),
361 together with *P. bulloides* and *E. trigona* (Figs. 3 and S2). Living *B. aculeata* have a widespread distribution,
362 with a preference for water depths ranging from 1500 to 2500m, and are typically associated with high organic
363 carbon fluxes (Mackensen et al., 1995; Almogi-Labin et al., 2000; Caille et al., 2015). *P. bulloides* is a shallow
364 infaunal species, which prefers mesotrophic environments and shows adaptability with respect to oxygen
365 concentration in the Arabian Sea (Gupta and Thomas, 1999; Caille et al., 2015). *E. trigona* is commonly
366 recorded in low oxygen habitats (Caille et al., 2015). We thus interpret assemblage 1 as indicating relatively
367 low-oxygen and meso- to eutrophic bottom water conditions during the late Holocene (6-1.4 cal kyr BP).

368 However, the lower oxygen concentrations reflected by benthic fauna 1 seem to be the opposite of what would
369 be expected under an enhanced influence of better ventilated NADW in IDW during the Holocene in the
370 northern Indian Ocean. Thus, another process has to be explored to combine our observations. To do that, we can
371 use the relative abundance of *Globigerina bulloides*, a proxy of upwelling activity, that increased in the late
372 Holocene in core MD77-191, suggesting an increased productivity in the southeastern Arabian Sea (Bassinot et
373 al., 2011) (Fig. 5). This record is synchronous with the benthic foraminiferal assemblage 1 (during the late
374 Holocene). Thus, increased surface productivity during the late Holocene could have induced more organic
375 matter in the intermediate water, leading to depleted oxygen conditions. By contrast, benthic assemblages 2 and
376 3 (during the last deglaciation and early Holocene; 17-6 cal kyr BP) are associated with low *G. bulloides*
377 abundances, suggesting lower productivity in the southeastern Arabian Sea during this period (Bassinot et al.,
378 2011) and thus indicating that intermediate water masses were characterized by higher bottom water oxygen
379 conditions and a lower flux of organic matter. Therefore, all of these elements suggest that changes in primary
380 productivity seem to be an important factor impacting the distribution of benthic assemblages at core MD77-191
381 site, especially during the Holocene.

382 In order to examine the relationships between intermediate C_{d_w} and these different processes (surface
383 productivity and/or water mass ventilation) in the eastern Arabian Sea, we can compare the MD77-191 C_{d_w}
384 values with the relative abundance of *G. bulloides* and benthic foraminiferal assemblage analyses from the same
385 core MD77-191, together with the records for C_{org} and the *G. bulloides* percentage obtained from core SK237
386 GC04 (1245m, southeastern Arabian Sea, Naik et al., 2017) (Fig. 5). Indeed, the total organic carbon (C_{org}) could
387 also be used as a qualitative indicator of past productivity and/or bottom water ventilation changes (Naidu et al.,
388 1992; Canfield, 1994; Calvert et al., 1995; Naik et al., 2017). Despite a lower resolution for MD77-191 *H.*
389 *elegans* C_{d_w} records, when compared to the C_{org} and the *G. bulloides* percentage from core SK237 GC04, all of
390 them seem to exhibit similar trends at the long-time scale even though some small-scale discrepancies can be
391 observed at millennial time scales (Fig. 5). From the last deglaciation to the late Holocene, the C_{d_w} record
392 displays a significant shift from ~ 0.7 nmol/kg to about twice values of ~ 1.59 nmol/kg. The intermediate C_{d_w}
393 values are thus extremely high during the late Holocene and synchronous with the higher values of C_{org} and *G.*
394 *bulloides* percentage records. These observed similar trends suggest that the increased surface productivity at the
395 core site during the late Holocene is associated to higher intermediate C_{d_w} values. Besides, previous studies have
396 suggested that increased C_{d_w} values (>1 nmol/kg) could correspond to elevated surface productivity (Bostock et
397 al., 2010; Olsen et al., 2016). However, at millennial time scale, we also observed several decreases in
398 intermediate C_{d_w} values (~ 0.81 nmol/kg) during the late Holocene, reaching nearly similar values during the last
399 deglaciation (Fig. 5). Thus, the variations in the C_{d_w} values cannot be fully associated to variations in the surface
400 productivity.

401 As mentioned before, during the Holocene, an increased influence of NADW in IDW was observed in the
402 northern Indian Ocean (Yu et al., 2018; Ma et al., 2019; 2020). NADW is characterized by a depleted nutrient
403 content (modern C_{d_w} , ~ 0.2 nmol/kg; Poggemann et al., 2017), and its contribution to IDW may affect the
404 intermediate C_{d_w} by deep-water masses upwelling when flowing northward. However, during the late Holocene,
405 benthic foraminiferal assemblage 1 is associated to lower oxygen concentrations, which seem to be inconsistent
406 with an enhanced influence of better ventilated NADW in IDW in the northern Indian Ocean. Therefore, this
407 appearing discrepancy seems to indicate that deep-intermediate water masses variations is not an important

408 control during the Holocene in this area, although we could not fully exclude the influence of NADW in IDW at
409 millennial time scale. Moreover, there is no clear evidence for such a millennial-scale variability in the IDW
410 and/or NADW circulation in the studied area. Thus, we suggest the intermediate C_{d_w} at core MD77-191 site may
411 be mainly influenced by surface productivity, especially during the Holocene.

412 In the Bay of Bengal, the benthic assemblages of core MD77-176 suggest that the intermediate water masses
413 were characterized by oligotrophic to mesotrophic conditions and/or well-ventilated environments during the
414 Holocene (Ma et al., 2019), associated with much lower surface productivity (Fig. S4). This observation is in
415 agreement with low primary productivity during the Holocene reconstructed by the relative abundance of
416 coccolith species *Florisphaera profunda* from the same core MD77-176 in the northeastern BoB (Zhou et al.,
417 2020). In the modern ocean, Prasanna Kumar et al. (2001) indicate that primary productivity in the BoB is much
418 lower than in the Arabian Sea, the lower surface productivity resulting from the large freshwater input from river
419 and direct rainfall resulting from enhanced Indian Summer Monsoon precipitation (e.g., Vinayachandran et al.,
420 2002; Madhupratap et al., 2003; Gauns et al., 2005). Moreover, when we compare the average C_{d_w} value of core
421 MD77-176 from the BoB (~ 0.9 nmol/kg) with results from core MD77-191 in the Arabian Sea (~ 1.2 nmol/kg),
422 lower values, especially during the late Holocene, are in agreement with the benthic assemblages.

423 To sum up, variations in the benthic assemblages seem to be associated with changes in the deep-water mass
424 ventilation and/or organic matter flux, linked to surface productivity. The benthic foraminiferal fauna are
425 consistent with the C_{d_w} record of core MD77-191 particularly during the late Holocene (6-1.4 cal kyr BP). Thus,
426 our results seem to show that the C_{d_w} record is mainly controlled by changes occurring at the surface, especially
427 during the Holocene. However, at millennial time scales, such during the HS1 and YD, the percentages of
428 planktonic species *G. bulloides* from cores MD77-191 and SK237 GC04 all indicate modest paleo-productivity,
429 the opposite of what is suggested by the results of core MD77-191 C_{d_w} , and the C_{org} record obtained from core
430 SK237 GC04. This interval is also marked by enriched *G. ruber* $\delta^{18}O$ values, indicating a weaker monsoon and
431 reduced freshwater inputs (Naik et al., 2017). This apparent discrepancy may be related to changes in the
432 intermediate water mass sources and/or ventilation during the last deglaciation.

433 So, in the next sections, we discuss i) processes controlling surface productivity and ii) changes in the
434 intermediate water circulation, both of them being potential drivers of the observed variations.

435

436 **5.3. Relationships between primary productivity and monsoon intensity**

437

438 During the Holocene, the intermediate water C_{d_w} records obtained from cores MD77-191 and MD77-176
439 seem to display depleted values in the early Holocene, followed by an abrupt increasing trend at the middle
440 Holocene, and then reaching higher values on the average (despite a short-timescale variability) during the late
441 Holocene.

442 Of the two cores, core MD77-176, located in the northeastern BoB, shows the lowest intermediate C_{d_w} (down
443 to ~ 0.83 nmol/kg) during the 10-6 cal kyr BP time interval. Observations described above suggest that this low
444 in C_{d_w} resulted from low primary productivity and thus reduced fluxes of organic matter to the intermediate
445 depths. We attribute this evolution to monsoon variation. Indeed, the early Holocene Climate Optimum (10-6 cal
446 kyr BP) is characterized by enhanced monsoon precipitation (Marzin et al., 2013; Contreras-Rosales et al., 2014)
447 (Figs. 6d-f) that resulted in increased freshwater discharge from the Ganges-Brahmaputra river system and from

448 the Irrawaddy River. However, the distribution of chlorophyll in surface water of the western BoB suggests a
449 low annual productivity, indicating that the BoB is not significantly influenced by the riverine nutrient input
450 (Zhou et al., 2020). Thus, it is likely that this increase in fresh water drove pronounced ocean stratification in the
451 northeast BoB, which could impede the nutrient transfer from intermediate/deep layer to the euphotic upper
452 seawater column, and then inducing low productivity. A similar low in Cd_w values is observed in the
453 reconstructed intermediate water Cd_w record from core MD77-191 during the early Holocene, with values
454 descending to ~ 0.92 nmol/kg, in the 10-6 cal kyr BP time interval. These low values of intermediate Cd_w are
455 coeval with low surface productivity as recorded by the *G. bulloides* percentage and low values in C_{org} content
456 from SK237 GC04 in the Arabian Sea (Fig.5). These variations are also recorded in changes in benthic
457 assemblages, with the occurrence of assemblage 2 associated to high oxygen levels and an oligotrophic
458 environment (Fig. 3). Off the southern tip of India, we cannot reject the possibility that increased monsoon
459 precipitation and enhanced freshwater runoffs in the BoB during the early Holocene, inducing a stronger
460 stratification, could explain part of the decrease in surface primary productivity. Yet, at this site, another
461 explanation prevails which is related to the decrease of summer monsoon wind intensity that drives local Ekman
462 pumping. As shown by Bassinot et al. (2011), the productivity variations at the southern tip of India are inversely
463 related to the evolution of upwelling activity along the Oman Margin, to the west of the Arabian Sea. Based on a
464 data/model comparison, Bassinot et al. (2011) showed that this anti-correlation can be attributed to the northward
465 shift of the ITCZ when boreal summer insolation reached a maximum in the early Holocene (Fig. 6a); this ITCZ
466 location results in enhanced summer monsoon wind intensity and an increase in the associated Ekman pumping
467 in the west of the Arabian Sea, and along the Oman margin, while it weakens at the southern tip of India. This
468 process may thus induce a decrease in surface productivity in the southeastern Arabian Sea.

469 In addition, Naik et al. (2017) pointed out the co-existence of low productivity during the early Holocene in
470 the BoB and to the South of India, in agreement with our data that clearly show the impact of such a reduction of
471 surface primary productivity on the intermediate water Cd_w . These authors suggested a direct relationship
472 between intense monsoon rainfall and reduced surface productivity. However, the northeastern BoB received a
473 much larger amount of river input than the southern tip of India during the early Holocene (Marzin et al., 2013).
474 Thus, it seems reasonable to propose that the northeastern BoB is more affected by the salinity-related
475 stratification effect, while the southern tip of India is more affected by the decrease in wind intensity (Bassinot et
476 al., 2011) with enhanced stratification being potentially made stronger by an additional fresh-water effect,
477 although weaker than in the BoB. Ultimately, both climatic features (summer wind intensity and precipitation)
478 are directly under the control of monsoon evolution resulting from the orbital forcing of low latitude boreal
479 summer insolation.

480 By contrast, higher intermediate Cd_w values from core MD77-191 associated with higher *G. bulloides* relative
481 abundances and C_{org} from core SK237 GC04 during the 5.2-2.4 cal kyr BP time interval could indicate enhanced
482 productivity during the mid to late Holocene (Naik et al., 2017) (Fig. 5). To a lesser extent, this is also observed
483 in the records from the Northern BoB for the same time-period. These changes are consistent with the weakened
484 summer monsoon intensity, with less rainfall during the late Holocene, as observed in the BoB using core
485 MD77-176 seawater $\delta^{18}O$ and core SO188-342KL δD_{Alk-ic} records (Marzin et al., 2013; Contreras-Rosales et al.,
486 2014; Figs. 6e-f). In addition, this is also strongly supported by the $\delta^{13}C_{wax}$ records from the Lonar Lake over the
487 Indian continent (Sarkar et al., 2015; Fig. 6d) and a progressive increase in monsoon summer winds to the South

488 of India (Bassinot et al., 2011). These observations could also strongly support the hypothesis that the major
489 control on surface productivity is linked to monsoon evolution in the BoB and at the southern tip of the Arabian
490 Sea during the Holocene (Bassinot et al., 2011; Naik et al., 2017; Zhou et al., 2020).

491

492 **5.4. Millennial-scale changes in intermediate water circulation during the deglaciation**

493

494 During the last deglaciation, short events have been recorded at the site of core MD77-191 during the 16-15.2
495 (HS1) and 12.6-11 cal kyr BP (YD) time intervals (Fig. 5). The low Cd_w values in the MD77-191 record are
496 coeval with reductions of C_{org} in core SK237 GC04 during the HS1 and YD periods (Fig. 5). According to
497 previous studies, extremely high Cd_w values (>1 nmol/kg) were reported to have been associated with enhanced
498 surface productivity (Bostock et al., 2010; Olsen et al., 2016). However, the range of values of intermediate Cd_w
499 (0.58-0.85 nmol/kg, HS1; 0.5-0.8 nmol/kg, YD) from core MD77-191 during the last deglaciation is much lower
500 compared with the Holocene Cd_w values (>1 nmol/kg), and thus may be associated with other processes such as
501 a better ventilation, changes in the water mass source, and/or depleted surface productivity (Fig. 6). Significant
502 decreases in *G. bulloides* relative abundance of cores SK237 GC04 (Naik et al., 2017) and MD77-191 records
503 were observed from the HS1 to B-A (Bassinot et al., 2011), and thereafter slight increases occurred in the YD
504 (Fig. 5). These high values at both core sites during the HS1 and YD may indicate an enhanced surface
505 productivity during these intervals (Fig. 5). This should have led to increased intermediate Cd_w and organic
506 matter preservation under low oxygen concentration conditions during the HS1 and YD. However, despite a low
507 resolution for the MD77-191 Cd_w record during the last deglaciation, we do not observe high values of
508 intermediate Cd_w during the HS1 and YD (~ 0.7 nmol/kg) compared with the late Holocene (~ 1.59 nmol/kg),
509 especially at 16.5-16 cal kyr BP. Although we cannot fully discard the influence of surface productivity on the
510 intermediate Cd_w in these time intervals, this apparent discrepancy seems to provide another evidence for the
511 influence of changes in water masses and/or ventilation during the HS1 and YD, in line with previous studies
512 and proxies in the northern Indian Ocean (Bryan et al., 2010; Yu et al., 2018; Ma et al., 2019; 2020).

513 Moreover, an increase in benthic $\delta^{13}C$ values is observed during the HS1 and YD in the northern Indian Ocean
514 (e.g., Duplessy et al., 1984; Curry et al., 1988; Naqvi et al., 1994; Jung et al., 2009; Ma et al., 2019) (Fig. S3).
515 The increase in the different benthic $\delta^{13}C$ records during the HS1 and YD in the western Arabian Sea, Pacific
516 Ocean and BoB is interpreted as reflecting the northward expansion of AAIW (Pahnke and Zahn, 2005; Jung et
517 al., 2009; Ma et al., 2019) (Fig. S3). The decreased benthic-planktonic foraminiferal ^{14}C offset (B-P age)
518 obtained from marine sediment cores from the Arabian Sea and the Bay of Bengal during the same intervals
519 could confirm enhanced vertical mixing in the Southern Ocean (Bryan et al., 2010; Ma et al., 2019). The
520 transition in the ϵ_{Nd} and $\Delta^{14}C$ records during the deglaciation also indicates a strong northward penetration of
521 AAIW within the North Atlantic and Bay of Bengal (e.g., Cao et al., 2007; Pahnke et al., 2008; Pena et al., 2013;
522 Yu et al., 2018). In addition, during the HS1 and YD, a decrease in the $[CO_3^{2-}]$ record from core MD77-191 also
523 suggests the release of CO_2 from the deep ocean in the deglacial period through the expansion of AAIW (Ma et
524 al., 2020). These time intervals are associated with better ventilation in the Southern Ocean (e.g., Anderson et al.,
525 2009; Skinner et al., 2010), which led to enhanced vertical ventilation resulting in increased production of
526 intermediate water masses (AAIW) (Anderson et al., 2009).

527 As mentioned before, previous studies have suggested an enhanced northward flow of southern sourced

528 intermediate water mass AAIW, observed as well as in the Atlantic, Pacific and Indian Oceans during the last
529 deglaciation (e.g., Pahnke et al., 2008; Bryan et al., 2010; Poggemann et al., 2017; Yu et al., 2018; Ma et al.,
530 2019, 2020), indicating that the source of intermediate water masses may be partly the same in these oceans.
531 Thus, as the benthic $\delta^{13}\text{C}$ values collected from the north Indian Ocean could better constrain the influence of
532 AAIW in the two studied cores (Naqvi et al., 1994; Jung et al., 2009; Ma et al., 2019; 2020) (Fig. S3), we can
533 also compare the range values of AAIW Cd_w from both studied cores with data from Atlantic and Pacific Oceans
534 at intermediate water depth during the HS1 and YD (Cd_w , 0.3-0.9 nmol/kg; Umling et al., 2018; Valley et al.,
535 2017). Thereafter, we could get the ranges of Cd_w - $\delta^{13}\text{C}$ values of AAIW during these intervals, based on the
536 benthic $\delta^{13}\text{C}$ records in Indian Ocean (Naqvi et al., 1994; Jung et al., 2009; Ma et al., 2019; 2020), as well as
537 benthic Cd_w values from Pacific and Atlantic Oceans (Valley et al., 2017; Umling et al., 2018) at intermediate
538 water depths (Fig. 7). Unfortunately, the resolution of both intermediate Cd_w and benthic $\delta^{13}\text{C}$ from core MD77-
539 176 (northeastern BoB) are very low for the HS1 and YD events, making it difficult to extract reliable
540 information. Thus, we have decided to focus on the results from core MD77-191 (0.5-0.85 nmol/kg) during these
541 two time-intervals; these results are in good agreement with the collected dataset (Fig. 7). Thus, the benthic Cd_w
542 results provide new evidence for tracking the northern flow of AAIW in the northern Indian Ocean, which
543 increased during HS1 and the YD.

544 Taken together, Cd_w , B-P age offset, benthic $\delta^{13}\text{C}$, ϵ_{Nd} and $\Delta^{14}\text{C}$ records reported from the northern Indian
545 Ocean all suggest strong upwelling and enhanced northern flow of AAIW from the Southern Ocean during HS1
546 and the YD. Thus, the variations in these records can provide strong evidence for the hypothesis that Southern
547 Ocean upwelling played a vital role in the increase of atmospheric CO_2 in the deglacial period (Anderson et al.,
548 2009; Skinner et al., 2010, 2014). However, Kohfeld et al. (2005) suggested that although physical processes
549 (such as ventilation) are involved in the glacial-interglacial atmospheric CO_2 change, the biological pump may
550 also contribute nearly half of the observed changes of CO_2 during the glacial-interglacial transitions. As shown
551 above, the HS1 event is characterized by reduced surface productivity, as revealed by the lower percentage
552 values of *G. bulloides* in core MD77-191 (Bassinot et al., 2011) and by several studies of cores located in the
553 eastern and western Arabian Sea within the Oxygen Minimum Zone (e.g., Schulz et al., 1998; Altabet et al.,
554 2002; Ivanochko et al., 2005; Singh et al., 2006, 2011; Naik et al., 2017). This reduced productivity at a
555 millennial timescale suggests that the entire biological factory was related to the reduced monsoon intensity
556 during the North Atlantic Heinrich events (e.g., Singh et al., 2011; Naik et al., 2017). Thus, a weaker biological
557 production could also have contributed to the two-step increase of atmospheric CO_2 during the last deglaciation,
558 at least for the HS1 period.

559

560 6. Conclusions

561

562 Changes in benthic foraminiferal Cd/Ca and assemblages were reconstructed on core MD77-191 (1254 m
563 water depth) located off the southern tip of India, as well as on core MD77-176 (1375 m water depth) from the
564 northern BoB, in order to reveal the evolution of intermediate water circulation and paleo-nutrient changes in the
565 northern Indian Ocean since the last deglaciation. We reconstructed seawater Cd_w concentration by converting *H.*
566 *elegans* Cd/Ca. Benthic Cd/Ca ratios are mainly influenced by changes in surface productivity and intermediate-
567 bottom water ventilation.

568 Results indicate that assemblages 2 and 3, reflecting high bottom water oxygen conditions and a low flux of

569 organic matter, dominated between 17 and 6 cal kyr BP, corresponding to a poor productivity time-period. The
570 typical late Holocene assemblage indicates a relatively low-oxygen level and meso- to eutrophic deep-water
571 conditions, associated with high surface productivity. The early Holocene (10-6 cal ka BP) corresponds to a low
572 in productivity associated with depleted Cd_w in intermediate water. These observations seem to result from
573 enhanced monsoon precipitation and increased river inputs from the Himalayan Rivers, which led to more
574 marked stratification in the BoB and a reduction in primary and export productivity. At the southern tip of India,
575 the decrease in vertical mixing is also associated with a reduction in summer wind forcing resulting from the
576 northward displacement of ITCZ during summer (Bassinot et al., 2011). During the late Holocene (5.2-2.4 cal
577 kyr BP), the increased intermediate Cd_w concentrations of cores MD77-191 and MD77-176 indicate enhanced
578 surface productivity in the southeastern Arabian Sea and in the northeastern BoB, corresponding to weakened
579 monsoon intensity and rainfall, in agreement with other local records and reconstructions of the paleo-monsoon
580 strength. Thus, our results clearly show the strong control of intermediate water Cd_w during the Holocene by
581 orbitally-driven changes in summer monsoon productivity.

582 As far as millennial-scale variability is concerned, during the last deglaciation, decreased intermediate Cd_w
583 concentrations during HS1 and the YD are coeval with increased benthic $\delta^{13}C$, depletion in $[CO_3^{2-}]$ and
584 decreased B-P age offsets. These observations indicate that the low Cd_w values in intermediate water mainly
585 resulted from the increased northward flow of AAIW during HS1 and YD intervals. These signals also provide
586 strong evidence for the important role of enhanced Southern Ocean ventilation in the CO_2 increase during the
587 last deglaciation. The declined intermediate Cd_w obtained from southeastern Arabian Sea (Core MD77-191),
588 combined with the published eastern and western Arabian Sea paleo-productivity results, together provide
589 evidence for the important influence of decreased monsoon intensity at a millennial time scale during cold events
590 in the North Atlantic region, associated with the increase in atmospheric CO_2 during the last deglaciation.

591

592 **Data availability**

593 All data are given in Table 1 and supplementary materials Tables S1-S2.

594

595 **Supplement**

596 The supplement related to this paper is available online.

597

598 **Author contribution**

599 RM, SS, FB and CC developed the idea and interpreted the results. CC and FB supplied foraminifera samples.
600 RM did benthic foraminifera assemblage and geochemical analyses with the aide of FH and LL. ZY and LL
601 joined the discussion. All co-authors helped to improve the article.

602

603 **Competing interests**

604 The authors declare that they have no conflict of interest.

605

606 **Acknowledgements**

607 R. Ma gratefully acknowledges the China Scholarship Council for providing funding for her study in France.
608 The authors wish to thank one anonymous reviewer as well as André Bahr for useful suggestions and discussions

609 during the revision process. The research leading to this paper was funded by the French National Research
610 Agency under the "*Investissements d'avenir*" programme (Grant ANR-11-IDEX-0004-17-EURE-0006), and the
611 INSU-LEFE-IMAGO-CITRON GLACE project.

612

613 **References**

614

615 Almogi-Labin, A., Schmiedl, G., Hemleben, C., Siman-Tov, R., Segl, M., and Meischner, D.: The influence of
616 the NE winter monsoon on productivity changes in the Gulf of Aden, NW Arabian Sea, during the last 530ka
617 as recorded by foraminifera, *Marine Micropaleontology*, 40 (3), 295–319, 2000.

618 Altabet, M. A., Hoggins, M. J., and Murray, R. W.: The effect of millennial-scale changes in the Arabian Sea
619 denitrification on atmospheric CO₂, *Nature*, 415, 159–162, 2002.

620 Altenbach, A. V., Pflaumann, U., Schiebel, R., Thies, A., Timm, S., and Trauth, M.: Scaling percentages and
621 distributional patterns of benthic foraminifera with flux rates of organic carbon, *Journal of Foraminiferal*
622 *Research*, 29 (3), 173–185, 1999.

623 Anderson, R. F., Ali, S., Bradtmiller, L. I., Nielsen, S. H. H., Fleisher, M. Q., Anderson, B. E., and Burckle, L.
624 H.: Wind-driven upwelling in the Southern Ocean and the deglacial rise in atmospheric CO₂, *Science*, 323
625 (5920), 1443–1448, 2009.

626 Barse, K.: Seasonality of phytoplankton chlorophyll in the central and northern Arabian Sea, *Deep Sea Research*
627 *Part A Oceanographic Research Papers*, 34 (5), 713–723, 1987.

628 Barker, S., Greaves, M., and Elderfield, H.: A study of cleaning procedures used for foraminiferal Mg/Ca
629 paleothermometry, *Geochemistry Geophysics Geosystems*, 4 (9), 1–20, 2003.

630 Bassinot, F. C., Marzin, C., Braconnot, P., Marti, O., Mathienblard, E., Lombard, F., and Bopp, L.: Holocene
631 evolution of summer winds and marine productivity in the tropical Indian Ocean in response to insolation
632 forcing: Data-model comparison, *Climate of the Past*, 7 (3), 815–829, 2011.

633 Bauska, T. K., Baggenstos, D., Brook, E. J., Mix, A. C., Marcott, S. A., Petrenko, V. V., Schaefer, H.,
634 Severinghaus, J. P., and Lee, J. E.: Carbon isotopes characterize rapid changes in atmospheric carbon dioxide
635 during the last deglaciation, *Proceedings of the National Academy of Sciences*, 113(13), 3465–3470, 2016.

636 Beal, L. M., Field, A., and Gordon, A. L.: Spreading of Red Sea overflow waters in the Indian Ocean, *Journal of*
637 *Geophysical Research: Oceans*, 105 (C4), 8549–8564, 2000.

638 Bostock, H. C., Opdyke, B. N., and Williams, M. J. M.: Characterising the intermediate depth waters of the
639 Pacific Ocean using $\delta^{13}\text{C}$ and other geochemical tracers, *Deep-Sea Research I*, 57 (7), 847–859, 2010.

640 Boyle, E. A.: Manganese carbonate overgrowths on foraminifera tests, *Geochim. Cosmochim. Acta*, 63 (18),
641 353–353, 1983.

642 Boyle, E. A.: Cadmium: Chemical tracer of deepwater paleoceanography, *Paleoceanography*, 3 (4), 471–489,
643 1988.

- 644 Boyle, E. A.: Cadmium and $\delta^{13}\text{C}$ paleochemical ocean distributions during the stage 2 Glacial Maximum,
645 Annual Review of Earth and Planetary Sciences, 20 (1), 245–287, 1992.
- 646 Boyle, E. A. and Keigwin, L. D.: Deep circulation of the north Atlantic over the last 200,000 years: Geochemical
647 evidence, Science, 218 (4574), 784–787, 1982.
- 648 Boyle, E. A., Labeyrie, L., and Duplessy, J. C.: Calcitic foraminiferal data confirmed by cadmium in aragonitic
649 Hoeglundina: Application to the Last Glacial Maximum in the northern Indian Ocean, Paleoceanography, 10
650 (5), 881–900, 1995.
- 651 Boyle, E. A., Sclater, F., and Edmond, J. M.: On the marine geochemistry of Cadmium, Nature, 263 (5572), 42–
652 44, 1976.
- 653 Bryan, S. P. and Marchitto, T. M.: Testing the utility of paleonutrient proxies Cd/Ca and Zn/Ca in benthic
654 foraminifera from thermocline waters, Geochemistry, Geophysics, Geosystems, 11 (1), 2010.
- 655 Bryan, S. P., Marchitto, T. M., and Lehman, S. J.: The release of ^{14}C -depleted carbon from the deep ocean during
656 the last deglaciation: Evidence from the Arabian Sea, Earth and Planetary Science Letters, 298 (1), 244–254,
657 2010.
- 658 Burmistrova, I. I. and Belyaeva, N. V.: Bottom foraminiferal assemblages in the Deryugin Basin (Sea of
659 Okhotsk) during the past 26000 years, Oceanology, 46 (6), 834–840, 2006.
- 660 Came, R. E., Oppo, D. W., Curry, W. B., and Lynch-Stieglitz, J.: Deglacial variability in the surface return flow
661 of the Atlantic meridional overturning circulation, Paleoceanography, 23, PA1217, 2008.
- 662 Canfield, D. E.: Factors influencing organic carbon preservation in marine sediments, Chem. Geol., 114, 315–329,
663 1994.
- 664 Calvert, S. E., Pedersen, T. F., Naidu, P. D., and von Stackelberg, U.: On the organic carbon maximum on the
665 continental slope of the eastern Arabian Sea, J. Mar. Res., 53, 269–296, 1995.
- 666 Cao, L., Fairbanks, R. G., Mortlock, R. A., and Risk, M. J.: Radiocarbon reservoir age of high latitude north
667 Atlantic surface water during the last deglacial, Quaternary Science Reviews, 26 (5), 732–742, 2007.
- 668 Caille, C., Mojtahid, M., Gooday, A. J., Jorissen, F. J., and Kitazato, H.: Living (rose-bengal-stained) benthic
669 foraminiferal faunas along a strong bottom-water oxygen gradient on the Indian margin (Arabian Sea),
670 Biogeosciences, 12 (16), 5005–5019, 2015.
- 671 Contreras-Rosales, L. A., Jennerjahn, T., Tharammal, T., Meyer, V., Lückge, A., Paul, A., and Schefuß, E.:
672 Evolution of the Indian Summer Monsoon and terrestrial vegetation in the Bengal region during the past 18
673 ka, Quaternary Science Reviews, 102, 133–148, 2014.
- 674 Corliss, B. H.: Recent deep-sea benthonic foraminiferal distributions in the southeast Indian Ocean: Inferred
675 bottom-water routes and ecological implications, Marine Geology, 31 (1-2), 115–138, 1979.

- 676 Corliss, B. H., Martinson, D. G., and Keffer, T.: Late Quaternary deep-ocean circulation, *Geological Society of*
677 *America Bulletin*, 97 (9), 1106, 1986.
- 678 Curry, W. B., Duplessy, J. C., Labeyrie, L. D., and Shackleton, N. J.: Changes in the distribution of $\delta^{13}\text{C}$ of deep
679 water σ_{CO_2} between the last glaciation and the Holocene, *Paleoceanography*, 3 (3), 317–341, 1988.
- 680 Curry, W. B., Ostermann, D. R., Guptha, M. V. S., and Ittekkot, V.: Foraminiferal production and monsoonal
681 upwelling in the Arabian Sea: evidence from sediment traps, *Geological Society, London, Special*
682 *Publications*, 64, 93–106, 1992.
- 683 De, S. and Gupta, A. K.: Deep-sea faunal provinces and their inferred environments in the Indian Ocean based
684 on distribution of recent benthic foraminifera, *Palaeogeography, Palaeoclimatology, Palaeoecology*, 291 (3),
685 429–442, 2010.
- 686 De Rijk, S., Jorissen, F. J., Rohling, E. J., and Troelstra, S. R.: Organic flux control on bathymetric zonation of
687 Mediterranean benthic foraminifera, *Marine Micropaleontology*, 40, 151–166, 2000.
- 688 Den Dulk, M., Reichart, G. J., Memon, G. M., Roelofs, E. M. P., Zachariasse, W. J., and Zwaan, G. J. V. D.:
689 Benthic foraminiferal response to variations in surface water productivity and oxygenation in the northern
690 Arabian Sea, *Marine Micropaleontology*, 35 (1–2), 43–66, 1998.
- 691 Duplessy, J. C., Shackleton, N. J., Matthews, R. K., Prell, W., Ruddiman, W. F., Caralp, M., and Hendy, C. H.:
692 ^{13}C record of benthic foraminifera in the last interglacial ocean: Implications for the carbon cycle and the
693 global deep water circulation, *Quaternary Research*, 21 (2), 225–243, 1984.
- 694 Eberwein, A. and Mackensen, A.: Live and dead benthic foraminifera and test $\delta^{13}\text{C}$ record primary productivity
695 off Morocco (NW-Africa), *Deep-Sea Research. Part I*, 53 (8), 1379–1405, 2006.
- 696 Eberwein, A. and Mackensen, A.: Last Glacial Maximum paleoproductivity and water masses off NW-Africa:
697 Evidence from benthic foraminifera and stable isotopes, *Marine Micropaleontology*, 67, 87–103, 2008.
- 698 Elderfield, H. and Rickaby, R. E. M.: Oceanic Cd/P ratio and nutrient utilization in the glacial Southern Ocean,
699 *Nature*, 405 (6784), 305–310, 2000.
- 700 Fontanier, C., Jorissen, F. J., Licari, L., Alexandre, A., Anschutz, P., and Carbonel, P.: Live benthic
701 foraminiferal faunas from the Bay of Biscay: Faunal density, composition, and microhabitats, *Deep Sea*
702 *Research Part I: Oceanographic Research Papers*, 49 (4), 751–785, 2002.
- 703 Gauns, M., Madhupratap, M., Ramaiah, N., Jyothibabu, R., Fernandes, V., Paul, J. T., and Prasanna Kumar, S.:
704 Comparative accounts of biological productivity characteristics and estimates of carbon fluxes in the Arabian
705 Sea and the Bay of Bengal, *Deep-Sea Research II*, 52, 2003–2017, 2005.
- 706 Gomes, H., Goes, J., and Saino, T.: Influence of physical processes and freshwater discharge on the seasonality
707 of phytoplankton regime in the Bay of Bengal, *Continental Shelf Research*, 20, 313–330, 2000.
- 708 Gupta, A. K. and Thomas, E.: Latest Miocene-Pleistocene productivity and deep-sea ventilation in the

- 709 Northwestern Indian Ocean (Deep Sea Drilling Project Site 219), *Paleoceanography*, 14(1), 62–73, 1999.
- 710 Gupta, A. K., Anderson, D. M., and Overpeck, J. T.: Abrupt changes in the Asian Southwest Monsoon during
711 the Holocene and their links to the North Atlantic Ocean, *Nature*, 421 (6921), 354–357, 2003.
- 712 Hammer, Ø., Harper, D. A. T., and Ryan, P. D.: Past: Paleontological statistics software package for education
713 and data analysis, 2001.
- 714 Hall, J. M. and Chan, L. H.: Ba/Ca in benthic foraminifera: Thermocline and middepth circulation in the north
715 Atlantic during the last glaciation, *Paleoceanography*, 19, PA4018, 2004.
- 716 Hermelin, J. O. R.: Relative abundances of benthic foraminifera in ODP hole 117-728A, *PANGAEA*, 1991.
- 717 Hermelin, J. O. R.: Variations in the benthic foraminiferal fauna of the Arabian Sea: A response to changes in
718 upwelling intensity? *Geological Society, London, Special Publications*, 64, 151–166, 1992.
- 719 Hermelin, J. O. R. and Shimmiel, G. B.: Impact of productivity events on the benthic foraminiferal fauna in the
720 Arabian Sea over the last 150,000 years, *Paleoceanography*, 10 (1), 85–116, 1995.
- 721 Hertzberg, J. E., Lund, D. C., Schmittner, A., and Skrivaneck, A. L.: Evidence for a biological pump driver of
722 atmospheric CO₂ rise during Heinrich Stadial 1, *Geophysical Research Letters*, 43(23), 12,242–12,251, 2016.
- 723 Hester, K. and Boyle, E.: Water chemistry control of Cadmium content in recent benthic foraminifera, *Nature*,
724 298, 260–262, 1982.
- 725 Holbourn, A., Henderson, A. S., and Macleod, N.: Front matter. In *Atlas of benthic foraminifera*, pp. 1–641,
726 2013.
- 727 Ivanochko, T. S., Ganeshram, R. S., Brummer, G. J. A., Ganssen, G., Jung, S. J. A., Moreton, S. G., and Kroon,
728 D.: Variations in tropical convection as an amplifier of global climate change at the millennial scale, *Earth
729 Planet. Sci. Lett.*, 235, 302–314, 2005.
- 730 Jaccard, S. L., Galbraith, E. D., Martínez-García, A., and Anderson, R. F.: Covariation of deep Southern Ocean
731 oxygenation and atmospheric CO₂ through the last ice age, *Nature*, 530(7589), 207–210, 2016.
- 732 Jones, R. W.: *The challenger foraminifera*, Oxford University Press, 1994.
- 733 Jung, S. J. A., Kroon, D., Ganssen, G., Peeters, F., and Ganeshram, R.: Enhanced Arabian Sea intermediate
734 water flow during glacial North Atlantic cold phases, *Earth and Planetary Science Letters*, 280 (1), 220–228,
735 2009.
- 736 Kohfeld, K. E., Quéré, C. L., Harrison, S. P., and Anderson, R. F.: Role of marine biology in Glacial-interglacial
737 CO₂ cycles, *Science*, 308, 74, 2005.
- 738 Laskar, L., Robutel, P., Joutel, F., Gastineau, M., Correia, A. C., and Levrard, B.: A long-term numerical
739 solution for the insolation quantities of the Earth, *Astronomy and Astrophysics*, 428, 261–285, 2004.

- 740 Lévy, M., Shankar, D., André, J.-M., Shenoi, S., Durand, F., and De Boyer Montegut, C.: Basin-wide seasonal
741 evolution of the Indian Ocean's phytoplankton blooms, *Journal of Geophysical Research*, 112 (C12014), 1–
742 14, 2007.
- 743 Loeblich, A. R. and Tappan, H.: Generic taxa erroneously regarded as foraminifers. In *Foraminiferal genera and*
744 *their classification*, Loeblich, A. R., Tappan, H., Eds. Springer US: Boston, MA, pp. 726–730, 1988.
- 745 Lynch-Stieglitz, J., Fairbanks, R. G., and Charles, C. D.: Glacial-interglacial history of Antarctic Intermediate
746 Water: Relative strengths of Antarctic versus Indian Ocean sources, *Paleoceanography*, 9 (1), 7–29, 1994.
- 747 Ma, R., Sépulcre, S., Bassinot, F., Haurine, F., Tisnérat-Laborde, N., and Colin, C.: North Indian Ocean
748 circulation since the last deglaciation as inferred from new elemental ratio records for benthic foraminifera
749 *Hoeglundina elegans*, *Paleoceanography and Paleoclimatology*, 35, 2020.
- 750 Ma, R., Sépulcre, S., Licari, L., Bassinot, F., Liu, Z., Tisnérat-Laborde, N., Kallel, N., Yu, Z., and Colin, C.:
751 Changes in intermediate circulation in the Bay of Bengal since the Last Glacial Maximum as inferred from
752 benthic foraminifera assemblages and geochemical proxies, *Geochemistry, Geophysics, Geosystems*, 20,
753 1592–1608, 2019.
- 754 Mackensen, A., Hubberten, H. W., Bickert, T., Fischer, G., and Futterer, D. K.: $\delta^{13}\text{C}$ in benthic foraminiferal
755 tests of *Fontbotia wuellerstorfi* (Schwager) relative to $\delta^{13}\text{C}$ of dissolved inorganic carbon in Southern Ocean
756 deep water: implications for Glacial ocean circulation models, *Paleoceanography*, 6, 587–610, 1993.
- 757 Mackensen, A., Schmiedl, G., Harloff, J., and Giese, M.: Deep-sea foraminifera in the South Atlantic Ocean;
758 ecology and assemblage generation, *Micropaleontology*, 41 (4), 342–358, 1995.
- 759 Madhupratap, M., Gauns, M., Ramaiah, N., Prasanna Kumar, S., Muraleedharan, P. M., Sousa, S. N., and
760 Muraleedharan, U.: Biogeochemistry of the Bay of Bengal: physical, chemical and primary productivity
761 characteristics of the central and western Bay of Bengal during summer monsoon 2001, *Deep-Sea Research*
762 II, 50, 881–896, 2003.
- 763 Marchitto, T. M. and Broecker, W. S.: Deep water mass geometry in the glacial atlantic ocean: A review of
764 constraints from the paleonutrient proxy Cd/Ca, *Geochemistry, Geophysics, Geosystems*, 7, 2006.
- 765 Marchitto, T. M., Lehman, S. J., Ortiz, J. D., Flückiger, J., and Geen, A. V.: Marine radiocarbon evidence for the
766 mechanism of deglacial atmospheric CO_2 rise, *Science*, 316, 1456–1459, 2007.
- 767 Marra, J. and Barber, R. T.: Primary productivity in the Arabian Sea: A synthesis of JGOFS data, *Progress in*
768 *Oceanography*, 65 (2), 159–175, 2005.
- 769 Marzin, C., Kallel, N., Kageyama, M., Duplessy, J. C., and Braconnot, P.: Glacial fluctuations of the Indian
770 monsoon and their relationship with north Atlantic climate: New data and modelling experiments, *Clim. Past*,
771 9 (5), 2135–2151, 2013.
- 772 McCorkle, D. C., Martin, P. A., W. Lea, D. W., and Klinkhammer, G. P.: Evidence of a dissolution effect on

- 773 benthic foraminiferal shell chemistry: $\delta^{13}\text{C}$, Cd/Ca, Ba/Ca, and Sr/Ca results from the ontong Java Plateau,
774 *Paleoceanography*, 10 (4), 699–714, 1995.
- 775 Mlénéck, V. M.: Sédimentation et dissolution des carbonates biogéniques aux moyennes latitudes Nord et Sud,
776 Approche quantitative et relations avec les paléocirculations océaniques des derniers 150 000 ans. PhD thesis,
777 Université Bordeaux I, pp. 277, 1997.
- 778 Monnin, E., Indermühle, A., Dällenbach, A., Flückiger, J., Stauffer, B., Stocker, T. F., Raynaud, D., and Barnola,
779 J. M.: Atmospheric CO₂ concentrations over the last glacial termination, *Science*, 291 (5501), 112–114, 2001.
- 780 Murgese, D. S. and De Deckker, P.: The distribution of deep-sea benthic foraminifera in core tops from the
781 eastern Indian Ocean, *Marine Micropaleontology*, 56 (1), 25–49, 2005.
- 782 Murgese, D. S. and De Deckker, P.: The late quaternary evolution of water masses in the eastern Indian Ocean
783 between Australia and Indonesia, based on benthic foraminifera faunal and carbon isotopes analyses,
784 *Palaeogeography, Palaeoclimatology, Palaeoecology*, 247 (3), 382–401, 2007.
- 785 Naqvi, W. A., Charles, C. D., and Fairbanks, R. G.: Carbon and oxygen isotopic records of benthic foraminifera
786 from the northeast indian ocean: Implications on glacial-interglacial atmospheric CO₂ changes, *Earth and*
787 *Planetary Science Letters*, 121 (1), 99–110, 1994.
- 788 Naidu, P. D., Prakash Babu, C., and Rao, C. M.: The upwelling record in the sediments of the western
789 continental margin of India, *Deep-Sea Res.*, 39, 715–723, 1992.
- 790 Naidu, P. D. and Malmgren, B. A.: A high-resolution record of late Quaternary upwelling along the Oman
791 margin, Arabian Sea based on planktonic foraminifera, *Paleoceanography*, 11, 129–140, 1996.
- 792 Naik, D. K., Saraswat, R., Lea, D. W., Kurtarkar, S. R., and Mackensen, A.: Last glacial-interglacial productivity
793 and associated changes in the eastern Arabian Sea, *Palaeogeography, Palaeoclimatology, Palaeoecology*, 483,
794 147–156, 2017.
- 795 O'Malley, R.: Ocean productivity. <http://www.science.oregonstate.edu/ocean.Productivity/index.php>. 2017.
- 796 Olsen, A., Key, R. M., van Heuven, S., Lauvset, S. K., Velo, A., Lin, X., and Suzuki, T.: The Global Ocean Data
797 Analysis Project version 2 (GLODAPv2) – an internally consistent data product for the world ocean, *Earth*
798 *System Science Data*, 8(2), 297–323, 2016.
- 799 Olson, D. B., Hitchcock, G. L., Fine, R. A., and Warren, B. A.: Maintenance of the low-oxygen layer in the
800 central Arabian Sea, *Deep-Sea Research Part II: Tropical Studies In Oceanography*, 40(3), 673–685. 1993.
- 801 Oppo, D. W. and Fairbanks, R. G.: Variability in the deep and intermediate water circulation of the Atlantic
802 Ocean during the past 25,000 years: Northern Hemisphere modulation of the Southern Ocean, *Earth and*
803 *Planetary Science Letters*, 86, 1–15, 1987.
- 804 Pahnke, K., Goldstein, S. L., and Hemming, S. R.: Abrupt changes in Antarctic Intermediate Water circulation
805 over the past 25,000 years, *Nature Geoscience*, 1, 870, 2008.

- 806 Pahnke, K. and Zahn, R.: Southern Hemisphere water mass conversion linked with north Atlantic climate
807 variability, *Science*, 307 (5716), 1741–1746, 2005.
- 808 Pena, L. D., Goldstein, S. L., Hemming, S. R., Jones, K. M., Calvo, E., Pelejero, C., and Cacho, I.: Rapid
809 changes in meridional advection of Southern Ocean intermediate waters to the tropical Pacific during the last
810 30kyr, *Earth and Planetary Science Letters*, 368, 20–32, 2013.
- 811 Peterson, L. C.: Recent abyssal benthic foraminiferal biofacies of the eastern Equatorial Indian Ocean, *Marine*
812 *Micropaleontology*, 8 (6), 479–519, 1984.
- 813 Phillips, S. C., Johnson, J. E., Giosan, L., and Rose, K.: Monsoon-influenced variation in productivity and
814 lithogenic sediment flux since 110 ka in the offshore Mahanadi Basin, northern Bay of Bengal, *Marine and*
815 *Petroleum Geology*, 58, 502–525, 2014.
- 816 Pichevin, L. E., Reynolds, B. C., Ganeshram, R. S., Cacho, I., Pena, L., Keefe, K., and Ellam, R. M.: Enhanced
817 carbon pump inferred from relaxation of nutrient limitation in the glacial ocean, *Nature*, 459(7250), 1114–
818 1117, 2009.
- 819 Poggemann, D. W., Hathorne, E., Nuernberg, D., Frank, M., Bruhn, I., Reißig, S., and Bahr, A.: Rapid deglacial
820 injection of nutrients into the tropical Atlantic via Antarctic Intermediate Water, *Earth and Planetary Science*
821 *Letters*, 463, 118–126, 2017.
- 822 Prasanna Kumar, S., Madhuratap, M., Dileep Kumar, M., Muraleedharan, P. M., de Souza, S. N., Gauns, M.,
823 and Sarma, V. V. S. S.: High biological productivity in the central Arabian Sea during the summer monsoon
824 driven by Ekman pumping and lateral advection, *Current Science*, 81, 1633–1638, 2001.
- 825 Prell, W. L. and Kutzbach, J. L.: Monsoon variability over the past 150,000 years, *Journal of Geophysical*
826 *Research Atmospheres*, 92 (D7), 8411–8425, 1987.
- 827 Reid, J. L.: On the total geostrophic circulation of the south Pacific Ocean: Flow patterns, tracers and transports,
828 *Progress in Oceanography*, 16 (1), 1–61, 2003.
- 829 Rostek, F., Bard, E., Beaufort, L., Sonzogni, C., and Ganssen, G. M.: Sea surface temperature and productivity
830 records for the past 240 kyr in the Arabian Sea, *Deep Sea Research Part II: Topical Studies in Oceanography*,
831 44(6-7), 1461–1480, 1997.
- 832 Saraswat, R., Nigam, R., and Correge, T.: A glimpse of the Quaternary monsoon history from India and
833 adjoining seas, *Palaeogeography, Palaeoclimatology, Palaeoecology*, 397, 1–6, 2014.
- 834 Sarkar, S., Prasad, S., Wilkes, H., Riedel, N., Stebich, M., Basavaiah, N., and Sachse, D.: Monsoon source shifts
835 during the drying mid-Holocene: Biomarker isotope based evidence from the core ‘monsoon zone’ (CMZ) of
836 India, *Quaternary Science Reviews*, 123, 144–157, 2015.
- 837 Schlitzer, R.: Ocean data view. <http://odv.awi.de>, 2015.

- 838 Schmiedl, G., De Bovee, F., Buscail, R., Charriere, B., Hemleben, C., Medernach, L., and Picon, P.: Trophic
839 control of benthic foraminiferal abundance and microhabitat in the bathyal Gulf of Lions, western
840 Mediterranean Sea, *Marine Micropaleontology*, 40, 167–188, 2000.
- 841 Schmiedl, G., Hemleben, C., Keller, J., and Segl, M.: Impact of climatic changes on the benthic foraminiferal
842 fauna in the Ionian Sea during the last 330,000 years, *Paleoceanography*, 13 (5), 447–458, 1998.
- 843 Schnitker, D.: Deep-sea benthic foraminifers: Food and bottom water masses. In: Zahn, R., Pedersent, T. F.,
844 Kaminski, M. A., Labeyrie, L. (eds), *Carbon cycling in the glacial ocean: Constraints on the ocean's role in*
845 *global change. NATO ASI Series (Series I: Global Environmental Change)*, vol 17, Springer, Berlin,
846 Heidelberg, 1994.
- 847 Schott, F. A. and McCreary, J. P.: The monsoon circulation of the Indian Ocean, *Progress in Oceanography*, 51,
848 1–123, 2001.
- 849 Schulz, H., von Rad, U., and Erlenkeuser, H.: Correlation between Arabian Sea and Greenland climate
850 oscillation of the past 110,000 years, *Nature*, 393, 54–57, 1998.
- 851 Shankar, D., Vinayachandran, P. N., and Unnikrishnan, A. S.: The monsoon currents in the north Indian Ocean,
852 *Progress in Oceanography*, 52(1):63–120, 2002.
- 853 Singh, A. D., Jung, S. J. A., Darling, K., Ganeshram, R., Ivanochko, T., and Kroon, D.: Productivity collapses in
854 the Arabian Sea during glacial cold phases, *Paleoceanography*, 26, PA3210, 2011.
- 855 Singh, A. D., Kroon, D., and Ganeshram, R.: Millennial scale variations in productivity and OMZ intensity in
856 the eastern Arabian Sea, *Journal of the Geological Society of India*, 68 (3), 369–377, 2006.
- 857 Skinner, L. C., Claire, W., Scrivner, A. E., and Fallon, S. J.: Radiocarbon evidence for alternating northern and
858 southern sources of ventilation of the deep Atlantic carbon pool during the last deglaciation, *PNAS*, 111 (15),
859 5480–5484, 2014.
- 860 Skinner, L. C., Fallon, S., Waelbroeck, C., Michel, E., and Barker, S.: Ventilation of the deep Southern Ocean
861 and deglacial CO₂ rise, *Science*, 328 (5982), 1147–1151, 2010.
- 862 Stuiver, M. and Grootes, P. M.: GISP2 oxygen isotope ratios, *Quaternary Research*, 53, 277–284, 2000.
- 863 Tachikawa, K. and Elderfield, H.: Microhabitat effects on Cd/Ca and $\delta^{13}\text{C}$ of benthic foraminifera, *Earth and*
864 *Planetary Science Letters*, 202, 607–624, 2002.
- 865 Tomczak, M., and Godfrey, J. S.: *Regional oceanography: An introduction*. Daya Publishing House, 2003.
- 866 Talley, L. D., Pickard, G. L., Emery, W. J., and Swift, J. H.: Preface. In *Descriptive physical oceanography*
867 (sixth edition), Academic Press: Boston, pp. 1–383, 2011.
- 868 Thushara, V. and Vinayachandran, P. N.: Formation of summer phytoplankton bloom in the northwestern Bay of

869 Bengal in a coupled physical-ecosystem model, *Journal of Geophysical Research: Oceans*, 121 (12), 8535–
870 8550, 2016.

871 Toggweiler, J. R.: Variation of atmospheric CO₂ by ventilation of the ocean’s deepest water, *Paleoceanography*,
872 14, 571–588, 1999.

873 Umling, N. E., Thunell, R. C., and Bizimis, M.: Deepwater expansion and enhanced remineralization in the
874 eastern equatorial Pacific during the Last Glacial Maximum, *Paleoceanography and Paleoclimatology*, 33,
875 563–578, 2018.

876 Valley, S., Lynch-Stieglitz, J., and Marchitto, T. M.: Timing of deglacial AMOC variability from a high-
877 resolution seawater Cadmium reconstruction: Timing deglacial upper amoc variability, *Paleoceanography*, 32,
878 1195–1203, 2017.

879 Vinayachandran, P. N., Murty, V. S. N., and Ramesh Bahu, V.: Observations of barrier layer formation in the
880 Bay of Bengal during summer monsoon, *Journal of Geophysical Research*, 107, 8018, 2002.

881 Van der Zwaan, G. J., Duijnste, I. A. P., Den Dulk, M., Ernst, S. R., Jannink, N. T., and Kouwenhoven, T. J.:
882 Benthic foraminifers: Proxies or problems? A review of paleoecological concepts, *Earth-Science Reviews*, 46
883 (1), 213–236, 1999.

884 Xie, R. C., Marcantonio, F., and Schmidt, M. W.: Deglacial variability of Antarctic Intermediate Water
885 penetration into the north Atlantic from authigenic Neodymium isotope ratios, *Paleoceanography*, 27,
886 PA3221, 2012.

887 You, Y.: Implications of the deep circulation and ventilation of the Indian Ocean on the renewal mechanism of
888 North Atlantic Deep Water, *Journal of Geophysical Research: Oceans*, 105, 23895–23926, 2000.

889 Yu, Z., Colin, C., Ma, R., Meynadier, L., Wan, S., Wu, Q., Kallel, N., Sepulcre, S., Dapoigny, A., and Bassinot,
890 F.: Antarctic Intermediate Water penetration into the northern Indian Ocean during the last deglaciation,
891 *Earth and Planetary Science Letters*, 500, 67–75, 2018.

892 Yu, J., Menviel, L., Jin, Z. D., Thornalley, D. J. R., Foster, G. L., Rohling, E. J., McCave, I. N., McManus, J. F.,
893 Dai, Y., Ren, H., He, F., Zhang, F., Chen, P. J., and Roberts, A. P.: More efficient North Atlantic carbon
894 pump during the Last Glacial Maximum, *Nat. Commun.*, 10, 2019.

895 Zhou, X., Duchamp-Alphonse, S., Kageyama, M., Bassinot, F., Beaufort, L., and Colin, C.: Dynamics of
896 primary productivity in the northeastern Bay of Bengal over the last 26 000 years, *Clim. Past*, 16, 1969–1986,
897 2020.

898 Ziegler, M., Diz, P., Hall, I. R., and Zahn, R.: Millennial-scale changes in atmospheric CO₂ levels linked to the
899 Southern Ocean carbon isotope gradient and dust flux, *Nature Geoscience*, 6, 457–461, 2013.

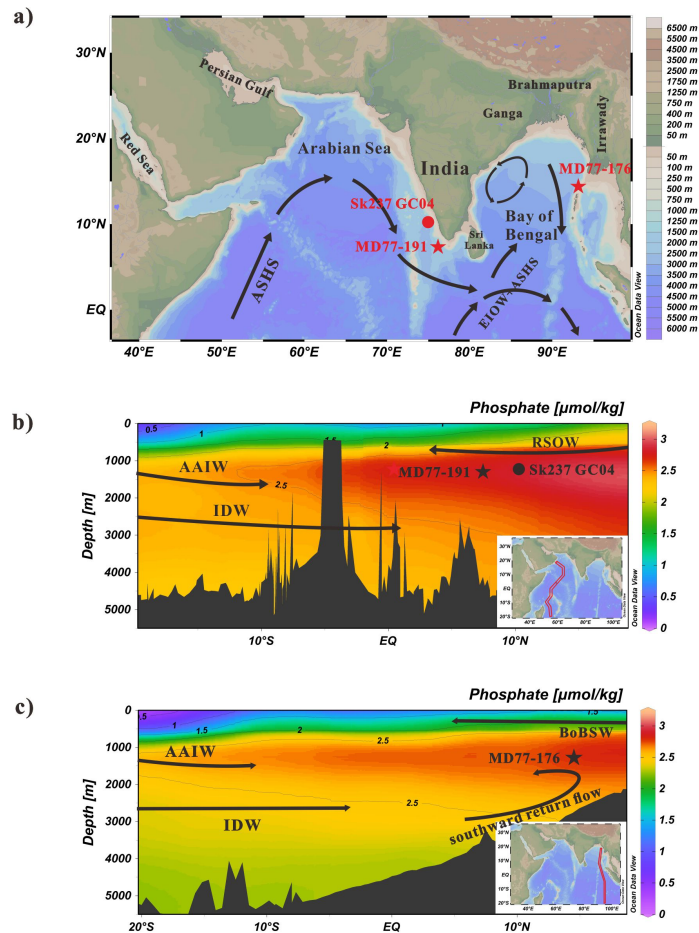
900

901

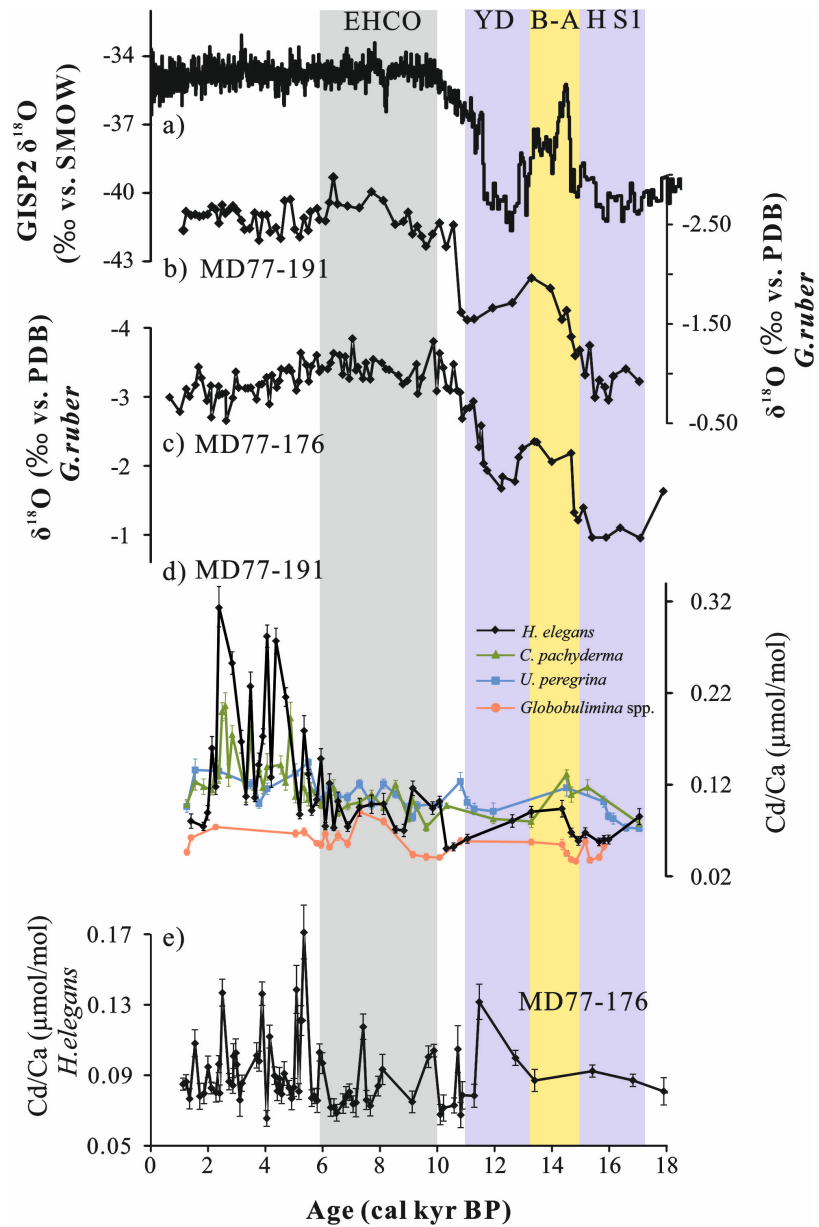
902

Table 1. Species composition of benthic foraminiferal assemblages from core MD77-191.

	Dominant species		Important associated species		Variance (%)
PC1					42
Positive loadings	<i>Bulimina aculeata</i>	0.84	<i>Pullenia bulloides</i>	0.18	
	<i>Cibicidoides pachyderma</i>	0.19	<i>Ehrenbergina trigona</i>	0.13	
Negative loadings	<i>Hoeglundina elegans</i>	-0.14	<i>Cibicidoides wuellerstorfi</i>	-0.04	
	<i>Bulimina manginata</i>	-0.07	<i>Globocassidulina subglobosa</i>	-0.06	
PC2					19
Positive loadings	<i>Sphaeroidina bulloides</i>	0.42	<i>Gyroidinoides orbicularis</i>	0.17	
	<i>Bulimina mexicana</i>	0.11	<i>Gyroidinoides soldanii</i>	0.07	
Negative loadings	<i>Bulimina aculeata</i>	-0.14	<i>Hoeglundina elegans</i>	-0.62	
	<i>Cibicidoides pachyderma</i>	-0.07			
PC3					8
Positive loadings	<i>Hoeglundina elegans</i>	0.66	<i>Globobulimina</i> spp.	0.22	
Negative loadings	<i>Uvigerina peregrina</i>	-0.59	<i>Cibicidoides pachyderma</i>	-0.21	

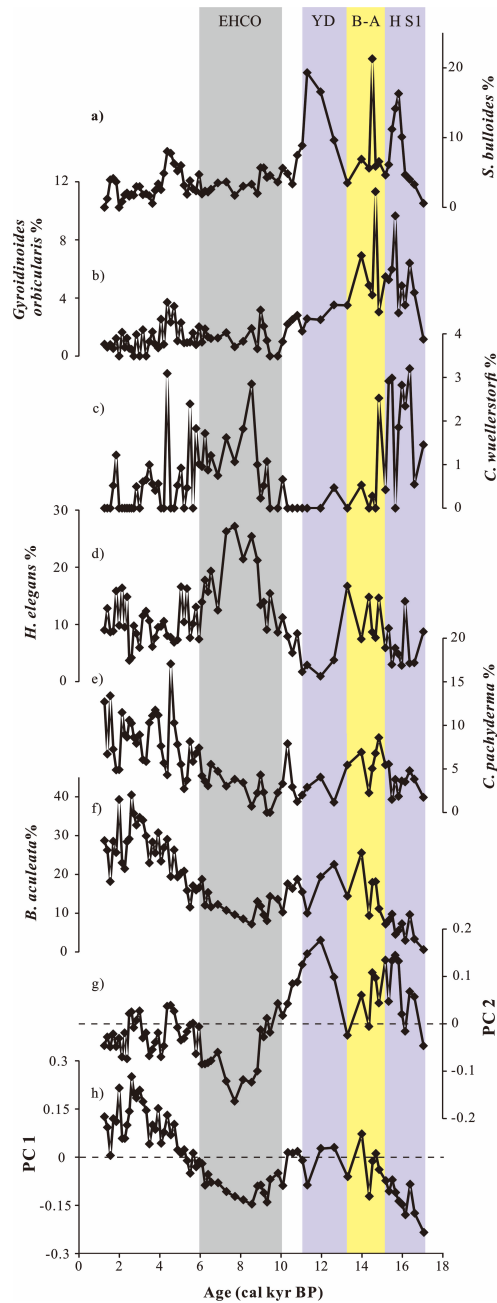


904
 905 **Fig. 1.** (a) Oceanographic setting and locations of core MD77-191 in the Arabian Sea (red star), core MD77-176
 906 in the Bay of Bengal (red star) and reference site SK237 GC04 (red circle, Naik et al., 2017). The black arrows
 907 represent the general surface circulation direction in the Northern Indian Ocean during the summer, Southwest
 908 Monsoon (Schott and McCreary, 2001). (b) and (c) Phosphate distribution along depth-latitude sections during
 909 the Southwest Monsoon and Northeast Monsoon periods, for the Arabian Sea and the Bay of Bengal,
 910 respectively. Data (in $\mu\text{mol/kg}$, colored scale) were contoured and plotted using the Ocean Data View (ODV)
 911 software (Schlitzer, 2015). On these two figures are shown the distribution and circulation of water masses in the
 912 Arabian Sea and Bay of Bengal (black arrows). ASHS: Arabian Sea High Salinity Water, EIOW: Eastern Indian
 913 Ocean Water, BoBSW: Bay of Bengal surface waters, AAIW: Antarctic Intermediate Water, RSOW: Red Sea
 914 Overflow Water, IDW: Indian Deep Water.
 915



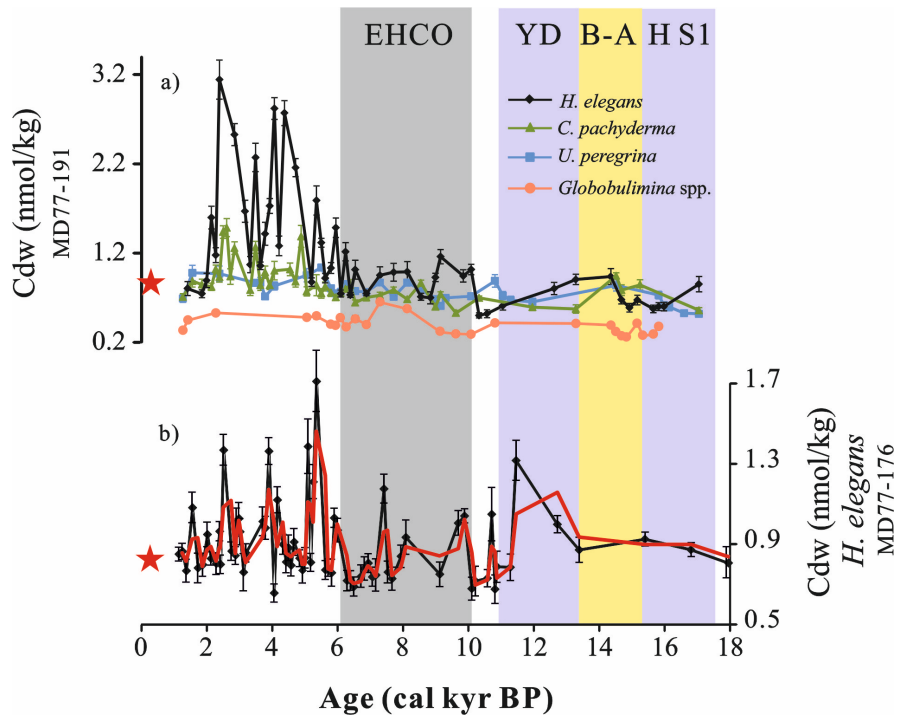
916
 917
 918
 919
 920
 921
 922
 923
 924

Fig. 2. (a) GISP2 Greenland ice core $\delta^{18}\text{O}$ signal (Stuiver and Grootes, 2000). (b)-(c) *Globigerinoides ruber* $\delta^{18}\text{O}$ records of cores MD77-191 and MD77-176, respectively (Marzin et al., 2013; Ma et al., 2020). (d) Cd/Ca records of the benthic foraminifera *Hoeglundina elegans* (black), *Cibicidoides pachyderma* (green), *Uvigerina peregrina* (blue), and *Globobulimina* spp. (orange) obtained from core MD77-191; (e) Cd/Ca records of the benthic foraminifera *H. elegans* from core MD77-176. EHCO for Early Holocene Climate Optimum, YD for Younger Dryas, B-A for Bølling-Allerød and HS1 for Heinrich stadial 1.



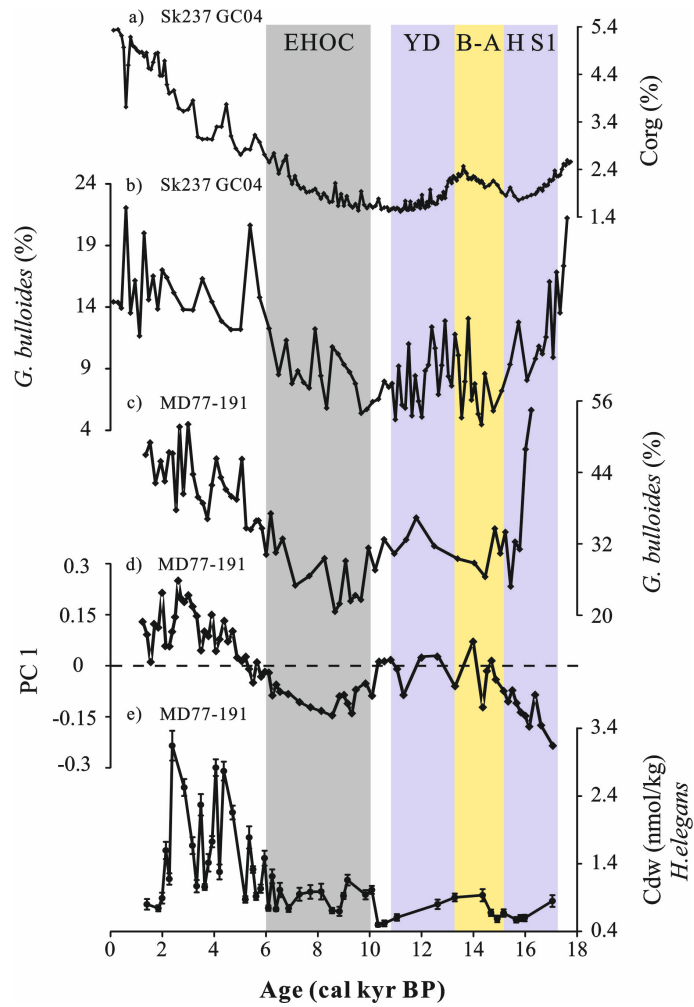
925
 926
 927
 928
 929
 930
 931

Fig. 3. Down core variations of PC scores and the percentages of major species. a) *Sphaeroidina bulloides* and b) *Gyroidinoides orbicularis* are dominated the assemblage 3, c) *Cibicoides wuellerstorfi* and d) *Hoeglundina elegans* are the main associated species of assemblage 2, e) *Cibicoides pachyderma* and f) *Bulimina aculeata* are major species in assemblage 1. The color shaded intervals and abbreviations are the same as in Figure 2.



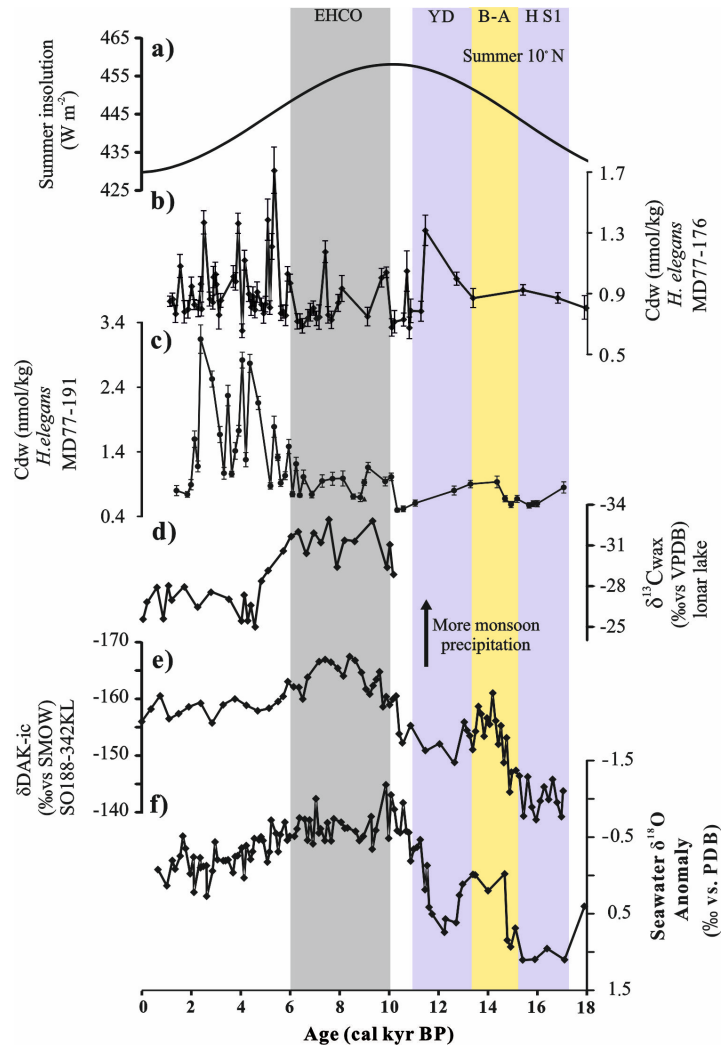
932
 933 **Fig. 4.** (a) Cd_w records calculated based on the Cd/Ca of benthic foraminifera *Hoeglundina elegans* (black),
 934 *Cibicoides pachyderma* (green), *Uvigerina peregrina* (blue), and *Globobulimina* spp. (orange) obtained from
 935 core MD77-191, (b) Cd_w record from core MD77-176 reconstructed using *H. elegans* Cd/Ca, the red line is the
 936 smoothed curves using a two-point moving average. The red stars represent the modern Cd_w (~0.83 nmol/kg) in
 937 the northern Indian Ocean (Boyle et al., 1995). The color shaded intervals and abbreviations are the same as in
 938 Figure 2.

939
 940
 941
 942



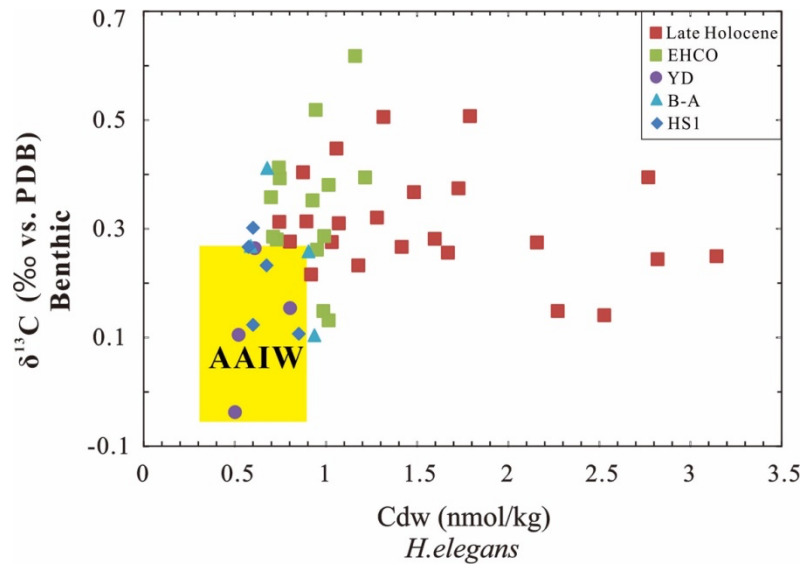
943
 944
 945
 946
 947
 948

Fig. 5. (a) Organic carbon weight percentage (%C_{org}) and (b) *G. bulloides* percentage from core SK237 GC04 (1245m, Arabian Sea, Naik et al., 2017). (c) Relative abundance of *G. bulloides* (Mlénéck, 1997; Bassinot et al., 2011), (d) PC 1 scores and (e) Cd_w records from core MD77-191 (Arabian Sea). The color shaded intervals and abbreviations are the same as in Figure 2.



949
 950
 951
 952
 953
 954
 955

Fig. 6. (a) The solar insolation at 10°N in summer (Laskar et al., 2004). (b) and (c) intermediate Cd_w calculated from *H. elegans* obtained from MD77-176 and MD77-191, respectively. (d) Lonar Lake $\delta^{13}C_{wax}$ record (Sarkar et al., 2015). (e) δD_{Alk-ic} record from core SO188-342KL (Contreras-Rosales et al., 2014). (f) Seawater $\delta^{18}O$ anomaly obtained from MD77-176 (Marzin et al., 2013). The color shaded intervals and abbreviations are the same as in Figure 2.



956
957

958 **Fig. 7.** Intermediate Cd_w versus benthic $\delta^{13}C$ obtained from core MD77-191 located off the southern tip of India.
959 The yellow shaded area represents the ranges of Cd_w - $\delta^{13}C$ values of AAIW during the HS1 and YD, which were
960 reconstructed in the Indian Ocean (benthic $\delta^{13}C$, Naqvi et al., 1994; Jung et al., 2009; Ma et al, 2019; 2020),
961 Pacific and Atlantic Oceans (benthic Cd_w , Valley et al., 2017; Umling et al., 2018) at intermediate water depths.
962 The abbreviations are the same as in Figure 2.